https://doi.org/10.5194/egusphere-2026-7224
Preprint. Discussion started: 27 November 2026
© Author(s) 2026. CC BY 4.0 License.

Modelled snow cover changes across Tyrol, Austria (1990–2023)

Elena Bertazza[1], Erwin Rottler[1], and Ulrich Strasser[1]
[1]Department of Geography, University of Innsbruck, Innsbruck, Austria
Correspondence: Elena Bertazza (elena.bertazza@uibk.ac.at)

Abstract. This study investigates changes in snow cover across Tyrol, Austria, between October 1990 and September 2023 based on simulations performed with the snow-hydrological model openAMUNDSEN. The model was driven by observations from a dense network of automatic weather stations and employed an energy balance snowmelt scheme. Model performance was assessed using in situ snow depth measurements and satellite-derived snow cover data. In addition, the simulated snow trends were compared with those obtained from SNOWGRID-CL, the climate version of GeoSphere Austria's operational snow model SNOWGRID. SNOWGRID-CL relies on an enhanced temperature-index approach and uses the SPARTACUS meteorological dataset as input. The openAMUNDSEN energy-balance-based simulation indicates pronounced interannual variability, but no statistically significant trends in snow water equivalent and snow depth over the investigated time period. Snow cover duration shows a decline across much of the study area, with statistically significant decreases in the eastern regions. In contrast, SNOWGRID-CL results show a more widespread and pronounced decrease in all variables. Differences between the two model outputs are primarily attributable to variations in meteorological forcing and are further amplified by differences in model complexity. Our energy-balance-based simulation further suggests that rising temperatures caused significant increases in the frequency surface snowmelt, wet-snow conditions and refreezing activity, particularly during winter and at high elevations. In high-alpine environments, the representation of liquid water retention and refreezing seems to be critical, as these processes can substantially affect model-based estimates of snow cover trends. Overall, our findings highlight the importance of high-quality meteorological forcing data for snow-hydrological modelling and demonstrate the value of physically based models for investigating snowpack responses to climate change.

1 Introduction

The accumulation and melt of seasonal snow cover play a fundamental role in Earth system processes, influencing climate, ecosystems, and hydrology. Snow cover strongly affects the land–atmosphere energy exchanges (Vavrus, 2007; Flanner et al., 2011), while the timing of spring snowmelt shapes the seasonal biological activity of plants and animals (Slatyer et al., 2022; Rumpf et al., 2022). At the soil level, snow cover regulates temperature and moisture conditions, thereby modulating microbial activity and nutrient cycling (Edwards et al., 2007). From a hydrological perspective, seasonal snow is a key freshwater source, particularly in mountainous regions and their downstream catchments (Viviroli et al., 2007; Rottler et al., 2021). Owing to orographic effects, mountainous regions generally receive more precipitation than adjacent lowlands, and their colder temperatures allow a substantial fraction of this precipitation to accumulate as snow. During spring, snowmelt releases this stored water

https://doi.org/10.5194/egusphere-2026-7224
Preprint. Discussion started: 27 November 2026
© Author(s) 2026. CC BY 4.0 License.

and sustains river runoff and reservoir recharge. Together with glacier melt during summer, this delayed release of freshwater ensures the water supply in many regions worldwide (DeWalle and Rango, 2008; Xiao et al., 2015; Immerzeel et al., 2020).

In recent decades, climate change has altered the meteorological conditions controlling snow accumulation and snow ablation (Auer et al., 2007; Beniston et al., 2018; Abram et al., 2019) and studies across mountain regions worldwide report reductions in snow cover duration (SCD), snow depth (SD) and snow water equivalent (SWE) since the mid-20th century (Marty et al., 2017; Hock et al., 2019; Matiu et al., 2021; Monteiro and Morin, 2023). In the European Alps, these declines are particularly pronounced in the southern sectors of the mountain range, at elevations below 1500 m, and during the seasonal transition from snow-covered to snow-free conditions (Valt and Cianfarra, 2010; Klein et al., 2016; Schöner et al., 2019; Matiu et al., 2021; Beaumet et al., 2021). Rising temperatures shift the 0 °C isotherm to higher elevations, causing precipitation to fall as rain rather than snow and resulting in pronounced changes at lower elevations (Dumont et al., 2025). Temperatures at higher elevations generally remain sufficiently low for precipitation to fall as snow (Scherrer et al., 2004; Bertoldi et al., 2023; Schöner et al., 2019). In terms of long-term variability, there is a broad agreement that a step-like regime shift occurred between the late 1980s and early 1990s (Marty, 2008; Reid et al., 2016). Although the precise timing varies with region and elevation, this shift has consistently been associated with a sharp decrease in SD, SCD and SWE (Laternser and Schneebeli, 2003; Durand et al., 2009; Valt and Cianfarra, 2010; Marty et al., 2017; Olefs et al., 2020; Colombo et al., 2022; Vorkauf et al., 2021; Ranzi et al., 2024). This abrupt decline was followed by a relatively stable period characterized by strong interannual variability and only weak trend signals (Colombo et al., 2022; Hüsler et al., 2014; Beaumet et al., 2021; Rumpf et al., 2022; Marty et al., 2017).

In general, the snow cover evolution can be investigated through in situ measurements, remote sensing and modelling (Dong, 2018). In situ observations provide accurate and long time series of key variables such as SD and SWE, but also more complex properties like density and liquid water content can be measured (Techel and Pielmeier, 2011; Pirazzini et al., 2018; Matiu et al., 2021; Warscher et al., 2024). High quality station observations allow for the detection of long-term trend signals (e.g. Marty and Meister, 2012; Bozzoli et al., 2024), however, they usually are limited to single or few point locations, making it hard to capture the full spatial variability across complex terrain. Remote sensing offers a broader spatial coverage and even investigations on a planetary scale are possible (e.g. Johnston et al., 2024; Dietz et al., 2015). Satellite-based snow data can complement in situ data, though the records are generally shorter and the measurements are subject to methodological constraints and limiting environmental factors, such as cloud cover or vegetation (Bormann et al., 2018; Demil et al., 2024). By comparison, snow model simulations can provide both continuous spatial and temporal estimates of snow conditions. Models range from simple empirical approaches to complex physically based frameworks that explicitly represent the energy and mass balance of the snowpack. Advanced snow model frameworks account for lateral snow redistribution processes and snow-canopy interaction and offer insights into the evolution of the snow cover on spatial and temporal scales that are difficult to capture from observations alone (Zhou et al., 2021). However, all snow model simulations go along with considerable level of uncertainty caused by simplified process representations, empirical parametrizations, and, most importantly, by the quality of the meteorological forcing data (Krinner et al., 2018; Günther et al., 2019; Günther et al., 2020; Rottler et al., 2026b). The combined use of in-situ measurements, remote sensing data, and snow modelling has become increasingly common in snow-

https://doi.org/10.5194/egusphere-2026-7224
Preprint. Discussion started: 27 November 2026
© Author(s) 2026. CC BY 4.0 License.

hydrological investigations, as it leverages the strengths of each data type and origin while compensating for their respective limitations (Dong, 2018; Wagner et al., 2026).

In this study, we assess characteristics and changes of the seasonal snow cover in Tyrol, Austria between October 1990 and September 2023. We perform fully distributed snow simulations with varying levels of process complexity, employing degree-day as well as energy balance approaches using the mountain snow-hydrological model openAMUNDSEN (Strasser et al., 2024). The snow simulations are forced by observations from a dense network of automatic weather stations (AWS) or by gridded meteorological products. To ensure the robustness of the modelling results, we evaluate model performance against station-based SD measurements as well as satellite-based snow data. In addition, we compare the simulations to SNOWGRID-CL results, a widely used snow data product for the region. Our analysis primarily focuses on the magnitude and statistical significance of trends in SD, SWE, and SCD. Furthermore, we investigate trends in internal snowpack processes, such as liquid water retention and refreezing, and examine their relationship with simulated snow cover trends.

2 Study area and Data

2.1 Study area

This study focuses on the federal state of Tyrol, located in Western Austria. Tyrol comprises two non-contiguous parts, North Tyrol and East Tyrol, which together cover approximately 12,650 km^2. The entire territory lies within the Eastern European Alps and is characterized by a typical Alpine landscape with alternating valleys, high peaks, glaciers, and mountain passes (Fig. 1). The largest valley in the region is the Inn Valley, shaped by the Inn River, which traverses much of North Tyrol along a southwest–northeast axis. The Inn River gathers runoff from numerous tributary valleys. Tyrol has more than 500 peaks exceeding 3,000 m a.s.l., the highest of which is the Großglockner (3,798 m a.s.l.), situated at the northeastern border of East Tyrol. Geologically, North Tyrol comprises a northern carbonate-dominated domain and a southern domain of predominantly igneous and metamorphic rocks. East Tyrol is characterized by alternating belts of gneisses, schists, and quartz-rich phyllites, with localized carbonate rocks in the south (GeoSphere Austria – Geological Map Service, 2026).

2.2 Data

We employed station observations from several regional data providers, including the national geological, geophysical, climatological and meteorological service of Austria (GeoSphere Austria), the Hydrographic Service of Tyrol (HD Tirol), the Avalanche Warning Service of Tyrol (LWD Tirol) and the Tiroler Wasserkraft AG (TIWAG). Using data from all major station operators in the region ensured the highest possible station density across elevations (Fig. 1 A,C). In addition, we included stations from neighbouring regions to improve the robustness of the simulations near the boundaries of the study area. Weather data from neighbouring regions in Austria were provided by GeoSphere Austria, while data from southern Germany were provided by the Bavarian Avalanche Warning Service (LWD Bayern). The station observations served as meteorological forcing for the snow-hydrological model simulations. Our snow surface energy-balance simulations require air temperature, precipita-

https://doi.org/10.5194/egusphere-2026-7224
Preprint. Discussion started: 27 November 2026
© Author(s) 2026. CC BY 4.0 License.

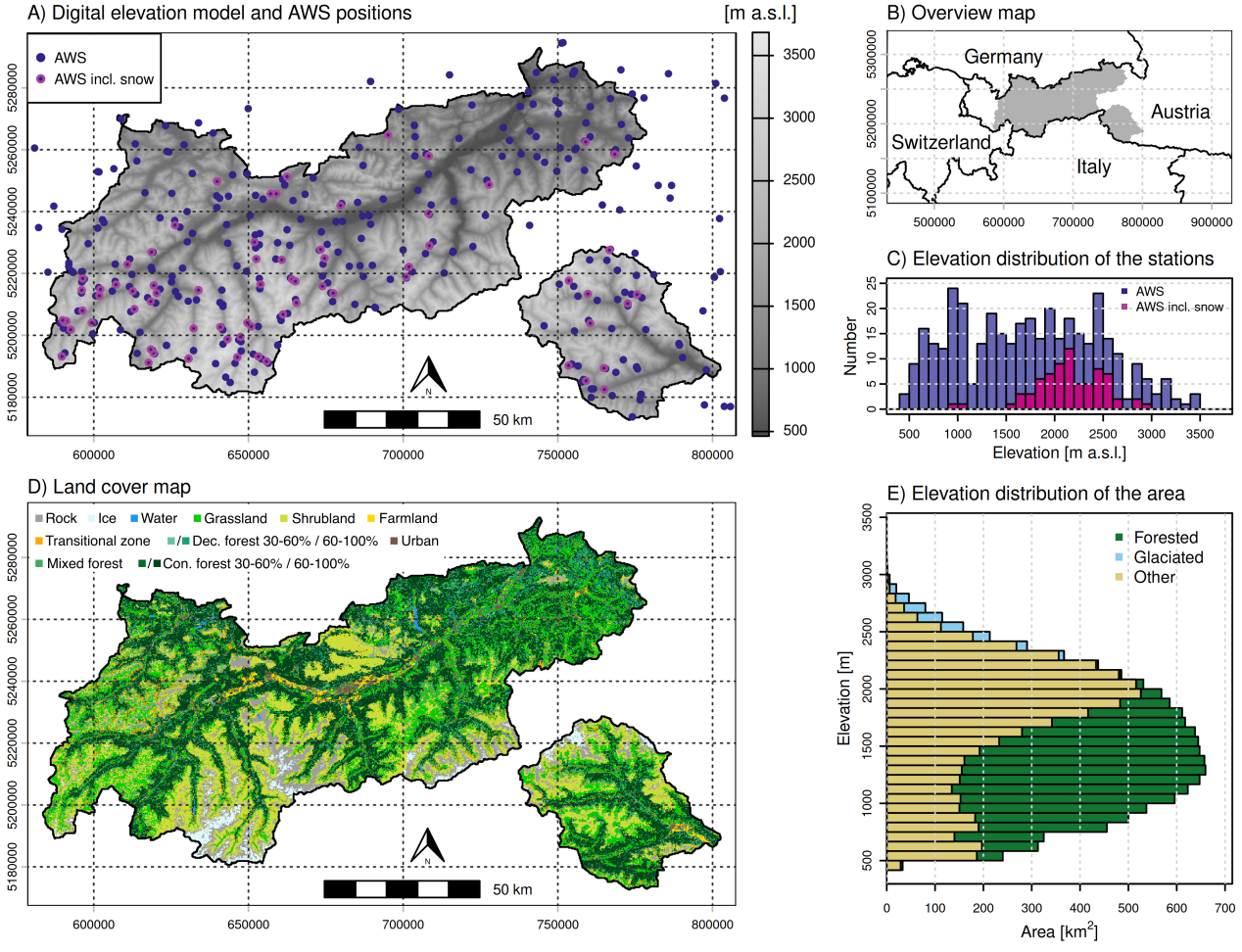

Figure 1. Digital elevation model of the study area including the locations of meteorological and snow stations (A), location of the federal state of Tyrol within Europe (B), elevation distribution of the meteorological stations (C), land cover/use based on the classification presented in Marsoner et al. (2023) (D), and the elevation distribution of the area including forest and glacier coverage (E). The station observations where provided by the national geological, geophysical, climatological and meteorological service of Austria (GeoSphere Austria), the Hydrographic Service of Tyrol (HD Tirol), the Tiroler Wasserkraft AG (TIWAG) and the Avalanche Warning Services of Tyrol (LWD Tirol) and Bavaria (LWD Bayern).

tion, relative humidity, incoming shortwave radiation and wind speed as forcing. We selected all stations that recorded at least one of these variables within the modelling period October 1990 to September 2023, resulting in a network of 372 meteorological stations. Because many stations had not yet been installed at the start of the modelling period and were established only later, the original records contain substantial temporal gaps, particularly early in the study period. A detailed overview of the pre-processing of station observations and the gap filling procedure applied to temperature and precipitation observations is

https://doi.org/10.5194/egusphere-2026-7224
Preprint. Discussion started: 27 November 2026
© Author(s) 2026. CC BY 4.0 License.

described in Section 3. In addition to meteorological forcing data, the snow model requires a digital elevation model (DEM) and a land cover map. The DEM was provided by the Federal state of Tyrol and can be downloaded on the Open Government Data Platform (https://www.data.gv.at/datasets/0454f5f3-1d8c-464e-847d-541901eb021a?locale=de; last access 04/03/2026). The spatial distribution of land cover classes is based on the land use/cover map developed within the EUSALP framework (Marsoner et al., 2023) (Fig. 1 D). We reclassified the original map to 13 land cover classes for the snow modelling with a particular focus on forest classes, as their representation is used to simulate snow-canopy interaction processes (Rottler et al., 2026b).

For comparison, we also collected the SPARTACUS v2.1 gridded meteorological data product developed by GeoSphere Austria. We downloaded and processed daily minimum and maximum air temperature as well as daily precipitation records (Hiebl and Frei, 2016, 2018; Hiebl et al., 2024). The SPARTACUS v2.1 dataset provides 1 km gridded data fields covering the entire country of Austria. These fields are derived from standard meteorological measurements and are freely available for download at the GeoSphere Austria Data Hub (https://data.hub.geosphere.at/dataset/spartacus-v2-1d-1km; last access 04/03/2026). In addition, daily maps of SD and SWE from the SNOWGRID-CL model were obtained for the snow model comparison. These gridded snow datasets also have a spatial resolution of 1 km and are freely available from the GeoSphere Austria Data Hub (https://data.hub.geosphere.at/dataset/snowgrid_cl-v2-1d-1km; last access 04/03/2026). SNOWGRID-CL is a distributed snow model that employs an enhanced temperature index approach for snowmelt calculation (Olefs et al., 2020; Pellicciotti et al., 2005). As meteorological forcing, it uses the SPARTACUS gridded data.

To evaluate the snow simulations against observations, we compiled two independent snow data sets. First, we processed in situ snow depth (SD) measurements from various data providers, comprising a total of 73 station records. The stations span an elevation range from 946 to 2,970 m a.s.l. (Fig. 1 A,C). Record lengths vary considerably, with the longest covering all winters of the study period and the shortest covering only the final winter. Then, to assess model performance in a spatially explicit manner, we used MODIS snow cover maps. Therefore, we downloaded and processed the Global SnowPack dataset from the German Aeorospace Center (DLR) (https://geoservice.dlr.de/; last access 04/03/2026). Global SnowPack provides daily maps in 500 m spatial resolution, and data gaps are filled by means of a step-wise temporal filter (Dietz et al., 2012, 2015; Roessler and Dietz, 2023). The daily data is available from 2000 onward.

3 Methods

3.1 Preprocessing of station data

In general, the meteorological data from GeoSphere Austria is of high quality, as the data processing at GeoSphere Austria is conducted in a standardized way including a series of quality checks. For higher frequency raw data from other providers, we aggregated to hourly values following the GeoSphere Austria's specifications. Accordingly, hourly air temperature corresponds to the value measured at the full hour and hourly precipitation is the sum accumulated over the preceding hour. Next, we applied basic quality tests to the hourly temperature time series. These included removing implausible high and low values using threshold checks and applying step-change and flatline filters. We also defined plausible temperature ranges depending

https://doi.org/10.5194/egusphere-2026-7224
Preprint. Discussion started: 27 November 2026
© Author(s) 2026. CC BY 4.0 License.

on elevation and time of the year and inspected values falling outside this temperature range. For precipitation, negative and unrealistically high values were removed from the raw time series prior to the aggregation to hourly totals. To ensure data reliability, we compared each hourly precipitation time series to the four nearest GeoSphere Austria precipitation records and computed the Pearson correlation coefficient between stations. Precipitation time series that showed a low correlation with all four neighbouring stations were flagged and not used as model forcing. An additional visual comparison of the neighbouring stations enabled us to identify further measurement errors. To address potential inhomogeneities in temperature and precipitation records (e.g. due to station relocations or instrument changes), we homogenized temperature and precipitation time series using the R package 'climatol' (Guijarro et al., 2023). This procedure was applied to all stations from HD Tirol, LWD Tirol and TIWAG, whereas the time series of GeoSphere Austria were not modified by the process. Temperature homogenization was performed on 357 records, identifying 135 break points across 88 stations. For precipitation, homogenization was performed on 215 records, identifying 22 break points across 17 stations. A similar preprocessing approach for temperature and precipitation was conducted in Rottler et al. (2026a), who used a subset of the station recordings to perform station-based trend analyses on the sub-seasonal scale.

An initial inspection of the raw incoming shortwave radiation data revealed that several time series exhibited a constant offset causing positive or negative recordings also during nighttime. To correct this sensor bias, we estimated the daily offset as the median of nighttime measurements for every day and subtracted it from all measurements of the corresponding day. Time series with large offsets were deemed erroneous and excluded from model forcing. Standard quality filters were then applied to remove physically implausible outliers, abrupt step-changes, and prolonged flatlines. Because flatlines typically occur at night, day and night periods were treated separately. All time series were visually inspected for signs of instrumental drift, which may develop as radiation sensors age over time. When summertime radiation peak decreased progressively over successive years, the most affected years were flagged and excluded from the model forcing. Finally, the high-frequency measurements were aggregated to hourly values. For relative humidity, we followed the procedure as for the other variables. We removed physically impossible values, abrupt step changes, and prolonged flatlines and inspected the time series for sensor drift. Even though the current version of the snow-hydrological model does not require wind direction as forcing, both wind speed and direction were preprocessed to remove unphysical values and flatlines, and subsequently aggregated into vector-averaged hourly values.

The AWS-based meteorological forcing obtained after the preprocessing contained substantial gaps, stemming both from the removal of erroneous measurements and many stations becoming operational only after the start of the study period. In general, gaps in individual time series are not an issue for the snow-hydrological model openAMUNDSEN. Its spatial interpolation routine simply uses all available measurements at each time step to generate the forcing fields. Initial test simulations indicated that sufficient data were available throughout the study period to perform this spatial interpolation; however, the resulting temperature trend maps exhibited pronounced spatial inhomogeneities. Such inhomogeneities can arise in long-term model runs when the input station network is not static but changes over time, with stations being added or removed during the modelling period. For example, the inclusion of a station midway through the modelling period can alter the interpolated temperature field in its vicinity. These changes can affect long-term trend signals. To minimize artefacts associated with the evolving station forcing network, we reconstructed temperature and precipitation using dedicated gap-filling procedures. We

https://doi.org/10.5194/egusphere-2026-7224
Preprint. Discussion started: 27 November 2026
© Author(s) 2026. CC BY 4.0 License.

used established random forest approaches to gap-fill temperature and precipitation records. Gap-filling methods based on random forests or regression trees have been successfully applied in numerous contexts, including the reconstruction of station measurements (Stekhoven and Bühlmann, 2012; Körner et al., 2018; Kang et al., 2019; Alejo-Sanchez et al., 2025). For temperature we first selected neighbouring stations with the highest correlations. We then trained several random forest models with the R package 'ranger' (Wright and Ziegler, 2017). The predictors included temperatures from the selected neighbouring stations, elevation differences, spatial coordinates, day of the year (DOY), and time of day. The models differed in the number and combination of neighbouring stations used. The models were then used to impute missing temperatures at the target station. We applied different models depending on the data availability of the neighbouring stations. Performance was evaluated by predicting left-out observations and comparing them with measurements. The explained variance consistently exceeded 90 %, even when only one neighbouring station was available, indicating a robust performance.

Precipitation gaps were filled using a similar random forest–based approach. However, the intermittent and highly variable nature of precipitation makes it considerably more challenging to predict than temperature, requiring more sophisticated approaches. Therefore, precipitation gap filling was performed using the R package 'reddPrec' (Huerta et al., 2025), which is specifically designed for reconstructing missing values in daily precipitation time series. Random forest models were trained on precipitation measurements aggregated to daily sums (considering only days with at least 80% data availability) and subsequently used to predict missing daily totals. As the snow-hydrological simulations require hourly precipitation input, the reconstructed daily values were temporally disaggregated. For each station and gap period, the nearest station with available observations was identified and its hourly precipitation fractions (i.e., the proportion of the daily total occurring within each hour) were calculated. These fractions were then multiplied by the corresponding predicted daily total, yielding to an hourly precipitation time series for the target station. As for temperature, the gap-filling procedure showed strong performance, with correlations between observations and predictions of approximately 0.9, indicating robust model skill.

SD measurements were first cleaned by removing negative and physically implausible values. All subsequent preprocessing was performed manually, involving the identification and removal of sudden increases in snow depth that were not supported by observed precipitation, as well as measurements exhibiting unnatural or oscillatory behaviour. Manual preprocessing was necessary due to the frequent occurrence of measurement errors, particularly during transitions between snow-covered and snow-free conditions, when grass growth can affect sensor readings.

3.2 Snow-hydrological modelling

The snow-hydrological simulations were carried out with openAMUNDSEN (v1.0.3) (Strasser et al., 2024; Hanzer et al., 2024), a fully distributed snow modelling framework designed to simulate the evolution of a seasonal snow cover in mountain regions. The model requires as input time series of the meteorological variables which are typically derived from station measurements. These local recordings are spatially interpolated across the study area using a combined regression–inverse distance weighting algorithm that accounts for elevation. Elevation is provided by a DEM whose grid spacing sets the spatial resolution of the simulations, typically between 10 and 1,000 m. Terrain attributes derived from the DEM such as slope and exposition are used to compute the incoming radiation, including effects such as terrain shading and multiple reflections

https://doi.org/10.5194/egusphere-2026-7224
Preprint. Discussion started: 27 November 2026
© Author(s) 2026. CC BY 4.0 License.

between the surface and clouds. The DEM is also used to compute the Snow Redistribution Factors (SRFs) based on the concept of topographic openness (Yokoyama, 2002) that account for the effects of wind- and gravity-driven processes that lead to preferential snow deposition in concave and erosion from convex areas (Hanzer et al., 2016). In addition, the model offers precipitation correction functions to account for gauge undercatch (Rasmussen et al., 2012; Kochendorfer et al., 2017).

Snowmelt can be simulated using three different approaches: temperature index, enhanced temperature index, and energy balance. In the temperature index method, snowmelt is calculated using an empirical linear relationship between average daily temperature and the snowmelt amount. This is the simplest approach and only requires daily temperature and precipitation as meteorological input. The enhanced temperature index approach extends the previous method by including a term that accounts for incoming shortwave radiation and albedo (Pellicciotti et al., 2005). This modification enables snowmelt calculations at sub-daily time steps and requires radiation measurements as an additional input variable. In the energy balance approach, snowmelt is computed by solving the surface energy balance equation. This method considers all relevant energy fluxes, including shortwave and longwave radiation, sensible and latent heat fluxes, soil heat flux, and the energy supplied to the snowpack by precipitation. Unlike the empirical temperature index methods, this approach is physically based and requires observations of temperature, precipitation, humidity, wind speed and radiation as input (Strasser, 2008; Strasser et al., 2024).

openAMUNDSEN can represent the snowpack using two alternative layering schemes: cryolayers and multilayer. In the cryolayers scheme, the snowpack is divided into four layers: ice, firn, old snow, and new snow. Layer thicknesses evolve during the simulation, and the transitions between layers are governed by snow density or age. In the multilayer scheme, the snowpack is divided into a specified number of layers (three in our case) without predefined physical properties. At each time step, the mass and energy balance equations are solved for every layer, accounting for temperature and liquid water content (Essery, 2015). Because this scheme explicitly resolves internal energy exchanges within the snowpack, it must be used together with the energy balance snowmelt approach. Fresh snow density is computed using a temperature-dependent parametrization (Anderson, 1976). Subsequent density changes are simulated using a formula that accounts for compaction and snow metamorphism (Anderson, 1976; Jordan, 1991). During snowmelt, water is added to the snowpack. Once the maximum liquid water holding capacity is exceeded, excess water drains and contributes to runoff (Essery, 2015; Strasser et al., 2024). Liquid water within the snowpack can also refreeze if sufficient energy is lost; however, this process is only represented when the energy balance approach is used.

In the model, a dedicated snow-canopy module describes the influence of vegetation on meteorological variables and snow processes. For this purpose, a land cover map of the study area is required. In forested areas, wind speed and radiation are reduced, while temperature fluctuations are reduced in their amplitude compared to open terrain. In forested areas, snow is intercepted and can sublimate from the canopy interception storage. These interactions are parametrized primarily through the effective Leaf Area Index, which characterizes the type of the vegetation (Strasser et al., 2011, 2024; Storebakken et al., 2025). Model outputs are provided as netCDF files containing three-dimensional arrays for each selected variable. The first two dimensions represent space (x–y, or longitude–latitude) and the third represents time. This structure enables analysis of spatial patterns by aggregating over time and of temporal evolution by aggregating over space.

https://doi.org/10.5194/egusphere-2026-7224
Preprint. Discussion started: 27 November 2026
© Author(s) 2026. CC BY 4.0 License.

Table 1. Summary of the key characteristics of the three openAMUNDSEN snow model configurations investigated in this study, including abbreviation, spatial resolution, time step, snowmelt method, layering scheme, and forcing data.

Configuration	Resolution	Time step	Snowmelt	Layering	Forcing data
EB-AWS	250 m	3 hours	Energy balance	multilayer	Automatic Weather Stations
TI-AWS	250 m	1 day	Temperature index	cryolayers	Automatic Weather Stations
TI-SPA	250 m	1 day	Temperature index	cryolayers	SPARTACUS

In this study, we used three configurations of the openAMUNDSEN snow model to assess the sensitivity of results to different forcing datasets and snowmelt methods, and to facilitate the comparison with SNOWGRID-CL data. The first configuration employs the multilayer scheme and energy balance approach (Essery, 2015; Strasser et al., 2024), and runs at a 3-hour time step on a 250 m grid with preprocessed hourly station data recordings serving as model forcing (EB-AWS). Given the large extent of the study area, this spatial resolution represents a compromise between spatial detail of the results and computational demands, such as runtime and output size. Next, we employed the temperature index scheme of openAMUNDSEN forced with daily mean air temperatures and daily precipitation totals from the preprocessed AWS data (TI-AWS). All the other settings were kept the same compared to the EB-AWS configuration. As a third model configuration, we used the temperature index scheme driven by temperature and precipitation from SPARTACUS v.2.1 (TI-SPA). This configuration was chosen to assess the impact of alternative forcing input data and to provide a snow model whose complexity and forcing data are comparable with SNOWGRID-CL. All the other settings were again kept the same compared to the other configurations.

3.3 Snow model evaluation

The performance evaluation was conducted using both SD measurements and satellite imagery. Snow station data enable the assessment of simulated SD over long periods but are limited to point locations. In contrast, satellite imagery provides spatially distributed information on snow cover extent. These data sources are complementary rather than interchangeable and were therefore both used. The evaluation was performed for both openAMUNDSEN (EB-AWS) and SNOWGRID-CL simulations using identical procedures. For the station-based evaluation, simulated time series of daily mean SD were compared with measured values at the corresponding snow monitoring site. From each pair of time series, the following evaluation metrics were computed:

$$\mathrm{BIAS} = \frac{1}{n}\sum_{i=1}^{n} \mathrm{SIM}_i - \mathrm{MEA}_i \tag{1}$$

$$\mathrm{RMSE} = \sqrt{\frac{1}{n}\sum_{i=1}^{n} (\mathrm{SIM}_i - \mathrm{MEA}_i)^2} \tag{2}$$

https://doi.org/10.5194/egusphere-2026-7224
Preprint. Discussion started: 27 November 2026
© Author(s) 2026. CC BY 4.0 License.

$$\mathrm{NSE} = 1 - \frac{\sum_{i=1}^{n} \left(\mathrm{SIM}_i - \mathrm{MEA}_i\right)^2}{\sum_{i=1}^{n} \left(\mathrm{SIM}_i - \overline{\mathrm{MEA}}\right)^2} \tag{3}$$

$$\mathrm{COR} = \frac{\sum_{i=1}^{n} (\mathrm{MEA}_i - \overline{\mathrm{MEA}})(\mathrm{SIM}_i - \overline{\mathrm{SIM}})}{\sqrt{\sum_{i=1}^{n} (\mathrm{MEA}_i - \overline{\mathrm{MEA}})^2} \sqrt{\sum_{i=1}^{n} (\mathrm{SIM}_i - \overline{\mathrm{SIM}})^2}} \tag{4}$$

where MEA_i and SIM_i are the measured and simulated snow depths on day i, $\overline{\mathrm{MEA}}$ and $\overline{\mathrm{SIM}}$ the mean of measured and simulated SDs, and n the number of observations. The BIAS quantifies systematic under- or overestimation, while the root mean square error (RMSE) reflects the average error magnitude. The Nash–Sutcliffe efficiency (NSE) evaluates the model's predictive skill relative to the mean of the observations, and the Pearson correlation coefficient (COR) captures the agreement in temporal dynamics between simulated and measured values. SD records cover different time periods because most monitoring stations were installed after the investigation period. Consequently, aggregating the metrics into single global values would give equal weight to time series of very different lengths. To avoid this, we did not aggregate the metrics into a single value. Instead, we analysed and visualized them while accounting for both time series length and station elevation. We produced weighted density plots, using time series length as weights, to provide an overall assessment of model performance. Limitations remain when using station-based SD measurements, because the grid-based model simulations cannot resolve small-scale topographic variability and processes.

We also evaluated snow simulations using MODIS-based satellite imagery. Because satellite imagery has limited capability to detect snow beneath forest canopies (Rittger et al., 2020), all forested cells were masked. Glaciated cells were also excluded, as satellite data often cannot reliably distinguish seasonal snow from firn and glacier ice due to the overlapping spectral signatures (Aberle et al., 2025). We obtained binary classes (snow-covered and snow-free) from simulations applying a fixed SD threshold of 2 cm. To enable a consistent comparison, openAMUNDSEN simulations (250 m resolution) and MODIS snow cover data (500 m) were resampled to the 1 km grid of SNOWGRID-CL using the nearest-neighbour method.

We conducted a pixel-by-pixel comparison between the binary observed and simulated daily snow cover maps. Given the binary nature of the maps, four possible outcomes can occur: true positive (TP), true negative (TN), false positive (FP), and false negative (FN). We counted the pixel in each category and used these counts to calculate the model accuracy:

$$\mathrm{ACC} = \frac{\mathrm{TP} + \mathrm{TN}}{\mathrm{TP} + \mathrm{TN} + \mathrm{FP} + \mathrm{FN}} \tag{5}$$

ACC is defined as the fraction of pixels correctly classified by the simulation and thus ranges from 0 and 1. To assess how model accuracy varies with elevation, we performed pixel-by-pixel comparisons across 27 elevation bands. The bands were defined using 100 m elevation intervals, except for the highest band, which includes all pixels above 3,000 m due to the limited number of pixels at these elevations. We then grouped and averaged these values by DOY, yielding a 366×27 accuracy matrix. This approach reveals how ACC varies both seasonally and across elevation.

https://doi.org/10.5194/egusphere-2026-7224
Preprint. Discussion started: 27 November 2026
© Author(s) 2026. CC BY 4.0 License.

Although the ACC metric captures the overall agreement between simulations and observations, it does not indicate whether the model over- or underestimates snow cover extent. To assess the error's direction, we computed the snow cover fraction bias. For each elevation band and observation day, the snow cover fraction was defined as the number of snow-covered pixels divided by the total number of pixels. The bias was then obtained as the difference between simulated and observed snow cover fractions. As in the ACC analysis, the resulting bias estimates were computed across elevations and DOY. In addition, we assessed the bias in total annual SCDs (October to September) by calculating the difference between simulated and observed SCD maps. We averaged results for elevation bands and year.

3.4 Snow model comparison and trend analyses

Next, we compared different snow model simulations to identify discrepancies and investigate their causes. We first analyzed domain-mean time series and long-term mean maps of SD and SWE derived from the openAMUNDSEN (EB-AWS) and SNOWGRID-CL simulations. The time series were compared to assess agreement between the models regarding interannual variability, while spatial differences were evaluated by subtracting the long-term mean SD and SWE fields of two simulations. The EB-AWS simulation contained 61 cells (0.03 % of the study area) where snow persists throughout the summer and accumulates over multiple years, resulting in artificial snow towers. These cells were excluded from the computation of the average time series.

Subsequently, we computed trend maps for mean SD, SWE and SCD for all snow model runs. Trends were estimated with the R package 'zyp' (Bronaugh and Werner, 2023), which implements prewhitened Sen's slope (Sen, 1968; Theil, 1950) and evaluates significance with the Mann–Kendall test (Mann, 1945; Kendall, 1975; McLeod, 2022). We applied the default prewhitening method of Wang and Swail (2002). Trends were considered statistically significant at the 5 % level ($p < 0.05$). As the reference window for the trend analysis, we considered both an extended winter season (November to April) and the full hydrological year (October to September). The extended winter period is consistent with the approach of Olefs et al. (2020), who analysed snow trends in Austria using SNOWGRID-CL. However, this temporal window may be too restrictive at high elevations, where snow cover persists beyond April. To account for this, we additionally analysed trends over the full hydrological year. The analysis of all snow model configurations allowed us to investigate how the selection of forcing dataset and snowmelt method influences the resulting simulated snow trends. To further characterize differences between the two forcing datasets (AWS-based and SPARTACUS), trends in meteorological variables relevant to the simulated snow quantities were analysed. Particular attention was given to snowfall, which directly influences snow accumulation and snow cover evolution. As snowfall is not a direct input to the snow model but is derived from precipitation through temperature-dependent phase partitioning, trends in both precipitation and air temperature were also analysed. All trends were computed for both the extended winter period and the full hydrological year.

We then examined the snowpack processes represented in the EB-AWS configuration in greater detail, focusing on snow variables that are not available in empirical snowmelt routines. These variables capture processes associated with liquid water retention and refreezing, extending our analysis beyond the bulk snow properties typically considered in snow modelling. Specifically, we analysed three process-based variables: melt days, wet snow days, and refreezing days. Melt days are defined

https://doi.org/10.5194/egusphere-2026-7224
Preprint. Discussion started: 27 November 2026
© Author(s) 2026. CC BY 4.0 License.

as the number of days on which at least 1 mm of snow melts at the snowpack surface. As snowmelt can only occur when snow is present, this variable is inherently linked to SCD; consequently, a reduction in SCD is likely to lead to fewer melt days. However, the number of melt days can also increase despite little or no change in SCD, indicating more frequent melt events that do not substantially shorten the snow season but instead promote liquid water storage within the snowpack, with the potential for subsequent refreezing. Accordingly, we defined wet snow days as the number of days on which the uppermost snow layer contained at least 1 mm of liquid water. We chose this threshold to ensure consistency with the melt days variable. In the default configuration of the multilayer scheme of openAMUNDSEN, the uppermost snow layer has a fixed thickness of 10 cm when the total SD exceeds 20 cm. In such situations, 1 mm of liquid water corresponds to 1 % volumetric liquid water content in this layer. We defined refreezing days as the number of days during which at least 1 mm of liquid water refroze within the snowpack. We computed trend maps for these variables over both the extended winter season and the full hydrological year. Additionally, we analysed trend magnitude and statistical significance across several elevation bands spanning 100 m, with the exception of the wider uppermost band, which encompasses all grid cells above 3000 m due to limited cell number.

In the final step, we analysed meltwater dynamics to illustrate the potential implications for overall water availability and runoff. Here, meltwater is defined as the amount of liquid water leaving the snowpack. This differs from surface snowmelt, the variable used to define melt days. We characterized meltwater dynamics using the centre of mass timing of annual flow (CT), a metric widely used in hydrological studies to assess shifts in the timing of snowmelt-driven runoff (Stewart et al., 2004; Roberts et al., 2018; Uzun et al., 2021). It represents a flow-weighted mean date and indicates when, on average, runoff occurs during a hydrological year. To investigate the spatial distribution of CT, we generated an annual average map and examined the elevation dependence of meltwater timing across the same elevation bands defined above. Finally, we computed the trend map over the full hydrological year and analysed how trend magnitude and statistical significance change with elevation.

4 Results

4.1 Snow model evaluation

The evaluation of openAMUNDSEN (EB-AWS) and SNOWGRID-CL snow simulations against in situ snow observations shows generally good agreement for most of the station records. Both simulations exhibit similar performance, with the density curves exhibiting broadly similar shapes and peak positions across the four evaluation metrics (Fig. 2). Large discrepancies between simulations and observations only involve a small subset of station records. The longest station records cover nearly the entire simulation period, although with some gaps, particularly during summer; whereas the shorter records cover only a few winter seasons. Examples of snow depth time series of different length and from different elevations are provided in Fig. 3.

Evaluation metrics comparing the simulations with satellite observations indicate that, in both models, ACC varies with elevation and DOY (Fig. 4 A,B). This pattern reflects the seasonal evolution of snow cover: ACC is highest when the landscape is nearly fully snow-covered or snow-free, and it declines during transitional periods with partial snow cover. Because the timing of these transition periods varies with elevation, the pattern exhibits a mountain-like shape. The lowest ACC occurs

https://doi.org/10.5194/egusphere-2026-7224
Preprint. Discussion started: 27 November 2026
© Author(s) 2026. CC BY 4.0 License.

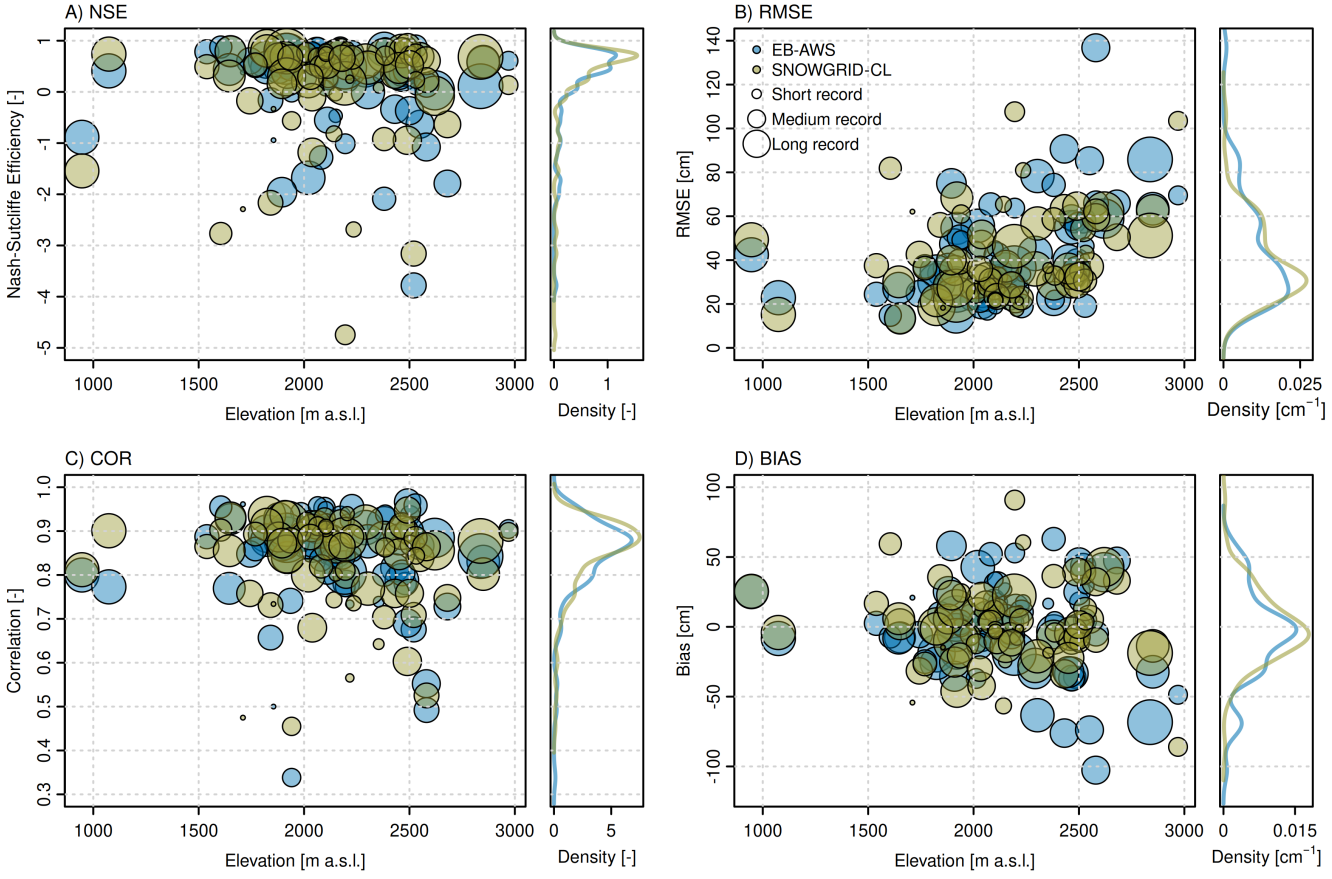

Figure 2. Evaluation of openAMUNDSEN (EB-AWS) and SNOWGRID-CL snow simulations using in situ snow observations (n = 73). In the density plots shown to the right of each panel, records are weighted by their respective lengths, with longer records assigned greater weight.

in SNOWGRID-CL, particularly in June between 1,700 and 2,500 m. When averaged across elevation bands, ACC exhibits a similar seasonal evolution in both models, with maxima in midwinter and minima in late spring and autumn.

The SCF BIAS pattern resembles that of ACC, with larger bias values corresponding to periods and elevation ranges with lower ACC. However, the sign and spatial distribution of the BIAS differ between the two models (Fig. 4 C,D). In EB-AWS, SCF is slightly overestimated across most elevation bands from January to April. Thereafter, a negative BIAS emerges near 1,500 m and intensifies with increasing elevation. From June onward, underestimation dominates the study area, with the strongest negative BIAS at the highest elevations. SNOWGRID-CL also exhibits a distinct BIAS pattern. From January to mid-March, snow cover fraction is generally underestimated at low elevations (below approximately 1,000 m) and overestimated elsewhere. During spring and early summer, a pronounced overestimation emerges, first appearing in mid-March at around 1,000 m and then progressively shifting to higher elevations (Fig. 4 D).

https://doi.org/10.5194/egusphere-2026-7224
Preprint. Discussion started: 27 November 2026
© Author(s) 2026. CC BY 4.0 License.

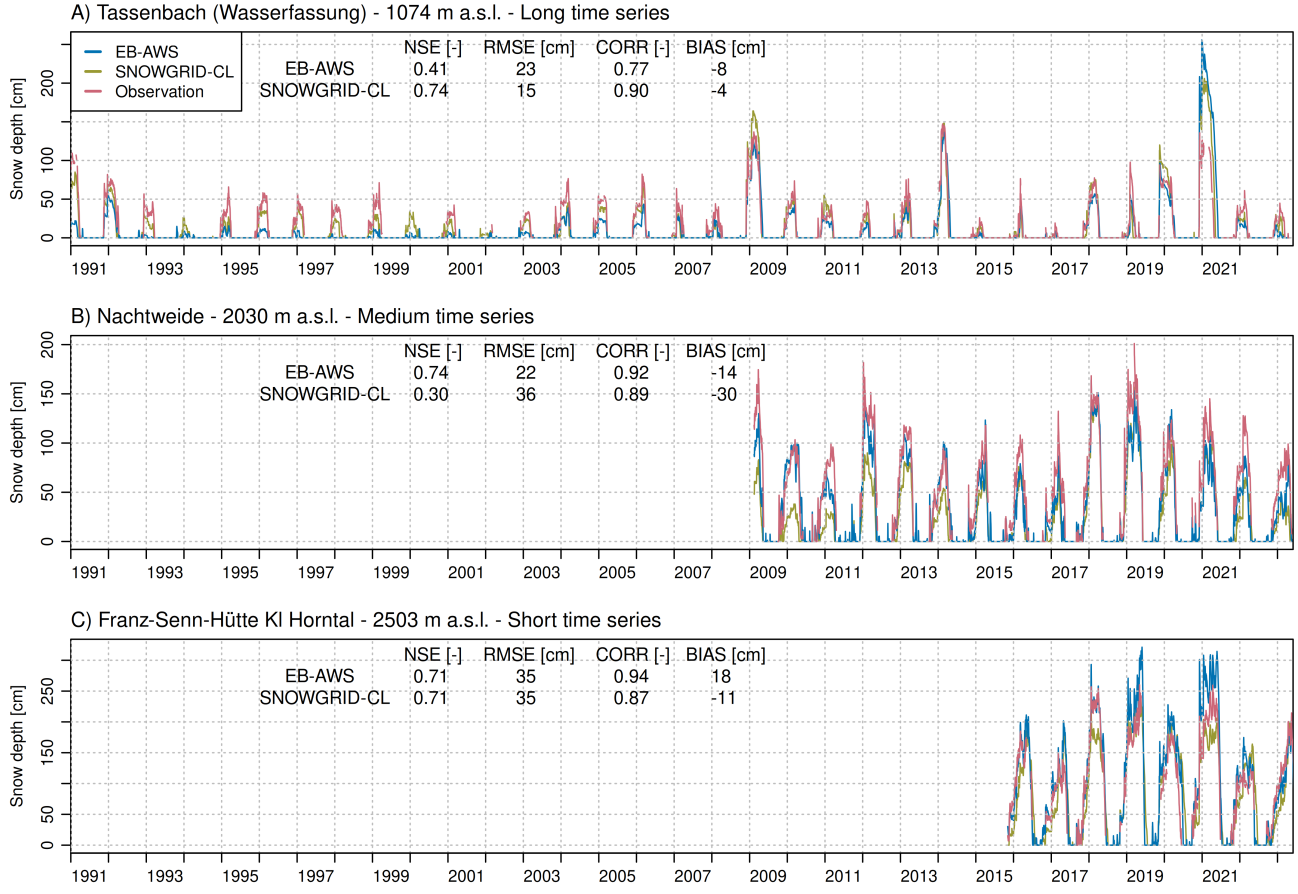

Figure 3. Selected simulated and observed snow depth time series illustrating long-, medium-, and short-term records at different elevations: (A) Tassenbach (Wasserfassung) (1,074 m a.s.l.), (B) Nachtweide (2,030 m a.s.l.), and (C) Franz-Senn-Hütte Kl Horntal (2,503 m a.s.l.). Evaluation metrics computed comparing observed and simulated values are provided for each station.

The BIAS in snow cover days (SCD) computed over the full hydrological year exhibits contrasting patterns in the two simulations (Fig. 4 E,F). In EB-AWS, the SCD BIAS is generally weakly positive at elevations below 2,500 m and negative at higher elevations. In contrast, SNOWGRID exhibits a negative bias below 1,000 m and a positive BIAS at higher elevations. Averaged across elevation bands, the SCD BIAS in EB-AWS remains close to zero with a standard deviation of about 5 days. SNOWGRID-CL exhibits a consistently positive BIAS of around 20 days per year, but with a standard deviation similar to that of EB-AWS.

4.2 Snow model comparison

We further examine differences between openAMUNDSEN (EB-AWS) and SNOWGRID-CL by comparing mean time series and spatial distributions of SD and SWE (Fig. 5, 6). Both models reproduce the strong interannual variability in SD and SWE

https://doi.org/10.5194/egusphere-2026-7224
Preprint. Discussion started: 27 November 2026
© Author(s) 2026. CC BY 4.0 License.

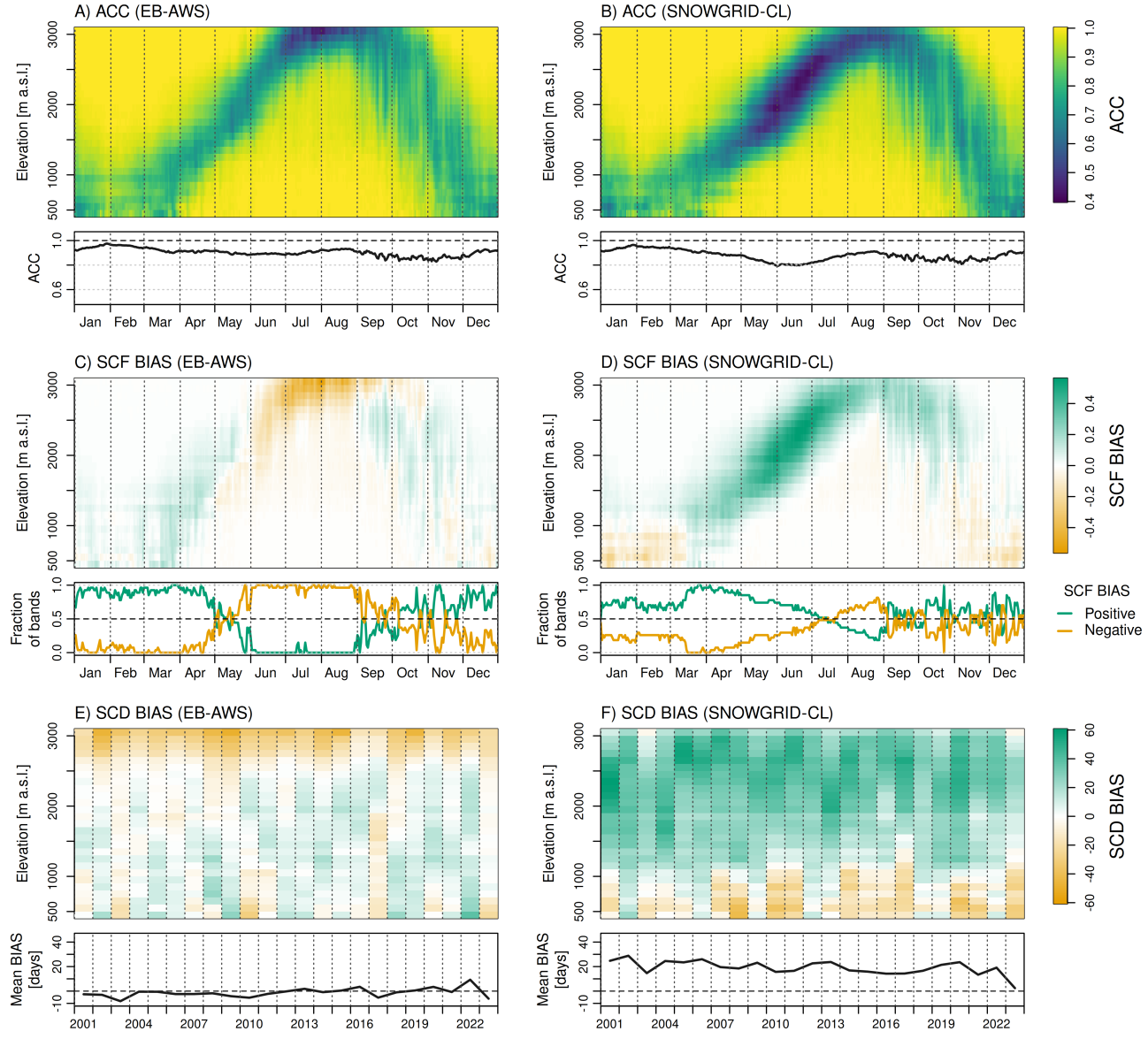

Figure 4. Evaluation of openAMUNDSEN (EB-AWS) and SNOWGRID-CL snow simulations against satellite-based MODIS snow-cover data for the period from October 2000 to September 2023: elevation- and season-dependent accuracy (ACC; A, B), elevation- and season-dependent biases in snow cover fraction (SCF; C, D), and elevation-dependent biases in snow cover duration (SCD) for hydrological years. Values were aggregated within 100 m elevation bands, with all grid cells above 3,000 m a.s.l. combined into a single elevation band.

and consistently identify snow-rich and snow-poor years (Fig. 5). Snow simulations indicate year-to-year variations exceeding 100 % in both SD and SWE. However, EB-AWS systematically simulates higher peak SWE values than SNOWGRID-CL,

https://doi.org/10.5194/egusphere-2026-7224
Preprint. Discussion started: 27 November 2026
© Author(s) 2026. CC BY 4.0 License.

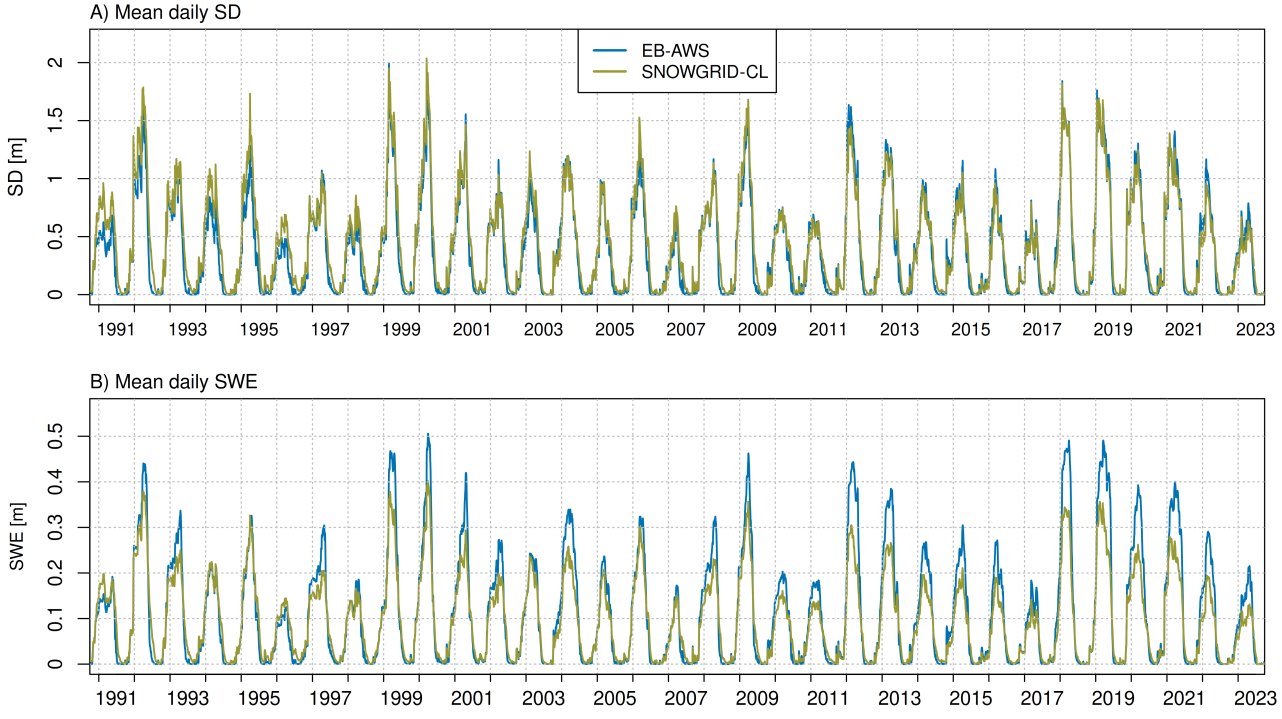

Figure 5. Comparison of domain-mean snow depth (SD; A) and snow water equivalent (SWE; B) across Tyrol, Austria, from October 1990 to September 2023, as simulated by openAMUNDSEN (EB-AWS) and SNOWGRID-CL.

while no comparable difference is evident for SD. Average maps also indicate higher SWE values in the EB-AWS simulations than in SNOWGRID-CL (Fig. 6). Differences in SD, by contrast, are less spatially consistent, although SNOWGRID-CL exhibits higher values across most of the study area.

The analysis of trend maps computed over the full hydrological year for selected snow variables indicates discrepancies between EB-AWS and SNOWGRID-CL (Fig. 7). Trend maps for the extended winter period are provided in the Appendix. Within each simulation run, the trend patterns for mean SWE and SD are broadly similar. EB-AWS results indicate a slight increasing tendency across the western part of the country and decreasing tendency in the east (Fig. 7 A, C). However, the these trends are generally not statistically significant. In contrast, SNOWGRID-CL suggests a decline in both variables across most of the study area, including significant negative trends in the westernmost regions (Fig. 7 B,D). Regarding SCD, EB-AWS indicates a significant decrease across the northeastern part of the study area, with maximum trend magnitudes of approximately 20 days decade^{-1}. In the western regions, trends are generally weaker, and statistically significant changes are confined to smaller areas. In contrast, SNOWGRID-CL indicates a strong and statistically significant decrease in SCD across most of the study area.

https://doi.org/10.5194/egusphere-2026-7224
Preprint. Discussion started: 27 November 2026
© Author(s) 2026. CC BY 4.0 License.

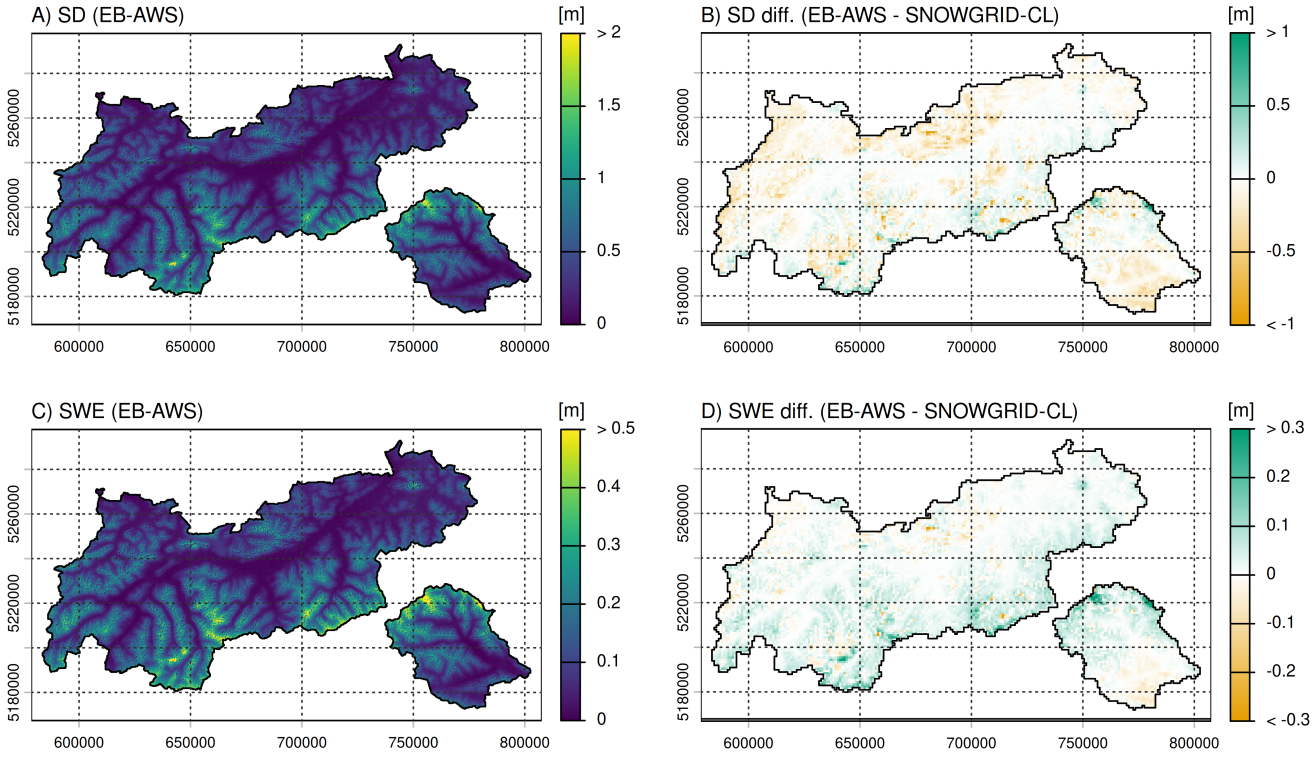

Figure 6. Maps of mean annual snow depth (SD; A) and snow water equivalent (SWE; C) for Tyrol, Austria, for the period from October 1990 to September 2023, simulated with openAMUNDSEN (EB-AWS). Panels B and D show the respective difference relative to SNOWGRID-CL.

The snow model configurations TI-AWS and TI-SPA both employ a temperature-index snowmelt scheme but differ in their meteorological forcing (Tab. 1). These two simulation experiments were designed to disentangle the effects of input data and model complexity on trends (Fig. 8). TI-AWS results exhibit trend patterns similar to EB-AWS; however, decreasing tendencies and SD and SWE and negative trends in SCD are more widespread and stronger over larger areas. TI-SPA yields trend patterns that generally align with those of SNOWGRID-CL.

The analysis of meteorological variables from the AWS-based dataset (used to force EB-AWS and TI-AWS) and SPARTACUS (used to force TI-SPA and SNOWGRID-CL) reveals contrasting spatial patterns in snowfall trends. In the AWS-based dataset, precipitation and snowfall trends exhibit broadly similar spatial distributions (Fig. 9 A,C), with decreasing trends in the eastern part of the study area and increasing trends in the west. Although precipitation trends are statistically significant in the western region, the corresponding snowfall trends are largely non-significant. In SPARTACUS, precipitation and snowfall trends show more pronounced spatial differences (Fig. 9 B,D). Precipitation trends are largely non-significant, whereas snowfall exhibits a statistically significant decrease in the northern part of the study area. Both datasets show statistically sig-

https://doi.org/10.5194/egusphere-2026-7224
Preprint. Discussion started: 27 November 2026
© Author(s) 2026. CC BY 4.0 License.

nificant warming across the entire study area (Fig. 9 E, F), with generally stronger temperature increases in SPARTACUS. This stronger warming may contribute to the divergence between precipitation and snowfall trends in SPARTACUS through temperature-dependent precipitation phase partitioning. The AWS-based precipitation trend map also exhibits spatial inhomogeneities, with localized patterns around individual station locations. These patterns may reflect local meteorological conditions that are not representative of the surrounding areas. In contrast, the SPARTACUS precipitation trend map shows fewer localized inhomogeneities, potentially reflecting the spatial smoothing applied in the construction of the data set.

4.3 Snowpack processes

The trend maps for SCD, melt days, wet snow days, and refreezing days reveal distinct patterns and levels of statistical significance depending on whether trends are calculated over the full hydrological year (left column) or over the extended winter season (right column) (Fig. 10,11). Over the full hydrological year, statistically significant increases in melt days are concentrated in elevations between 1,600 and 2,500 m a.s.l. (Fig. 10 C). In contrast, during the extended winter period, melt days increase significantly across all elevations above approximately 1,700 m a.s.l. (Fig. 10 D). Lower elevations exhibit a decrease in SCD for both analysis windows, particularly between 1,200 and 1,700 m a.s.l. (Fig. 10 C, D). Decreasing trends in SCD are more widespread when considering the full hydrological year because high elevation areas are fully covered by snow throughout the extended winter season.

The trends in wet snow days closely resemble those of melt days in terms of direction, spatial distribution and statistical significance (Fig. 11 A,B). Regarding refreezing days, the elevation zone exhibiting statistically significant increasing trends is shifted towards slightly higher elevations relative to melt and wet snow days (Fig. 11 C,D). The spatial trend patterns further points at the dependence of melt, wet snow, and refreezing days on the presence of snow. A reduction in SCD generally limits the number of days during which melt and refreezing processes can occur. Consequently, increases in melt, wet snow, or refreeze days only occur in areas where a declining SCD does not dominate the overall signal.

As expected, CT shows a clear elevation dependency, with meltwater being released earlier at lower elevations (Fig. 12 A). For example, the average CT occurs in mid-February for the 500–600 m elevation band, in mid-March for the 1,200–1,300 m elevation band, and progressively later at higher elevations. The CT trend map indicates that, over the study period, CT shifted to earlier dates across nearly the entire study area (Fig. 12 B). Statistically significant trends are largely confined to elevations between 1,800 and 2,500 m.

5 Discussion

5.1 Snow model evaluation

The evaluation of the openAMUNDSEN (EB-AWS) and SNOWGRID-CL outputs generally indicates good agreement with observations for both models, based on comparisons with in situ snow measurements and satellite imagery. The station-based evaluation indicates comparable performance for the two simulations. The few cases showing large differences between simu-

https://doi.org/10.5194/egusphere-2026-7224
Preprint. Discussion started: 27 November 2026
© Author(s) 2026. CC BY 4.0 License.

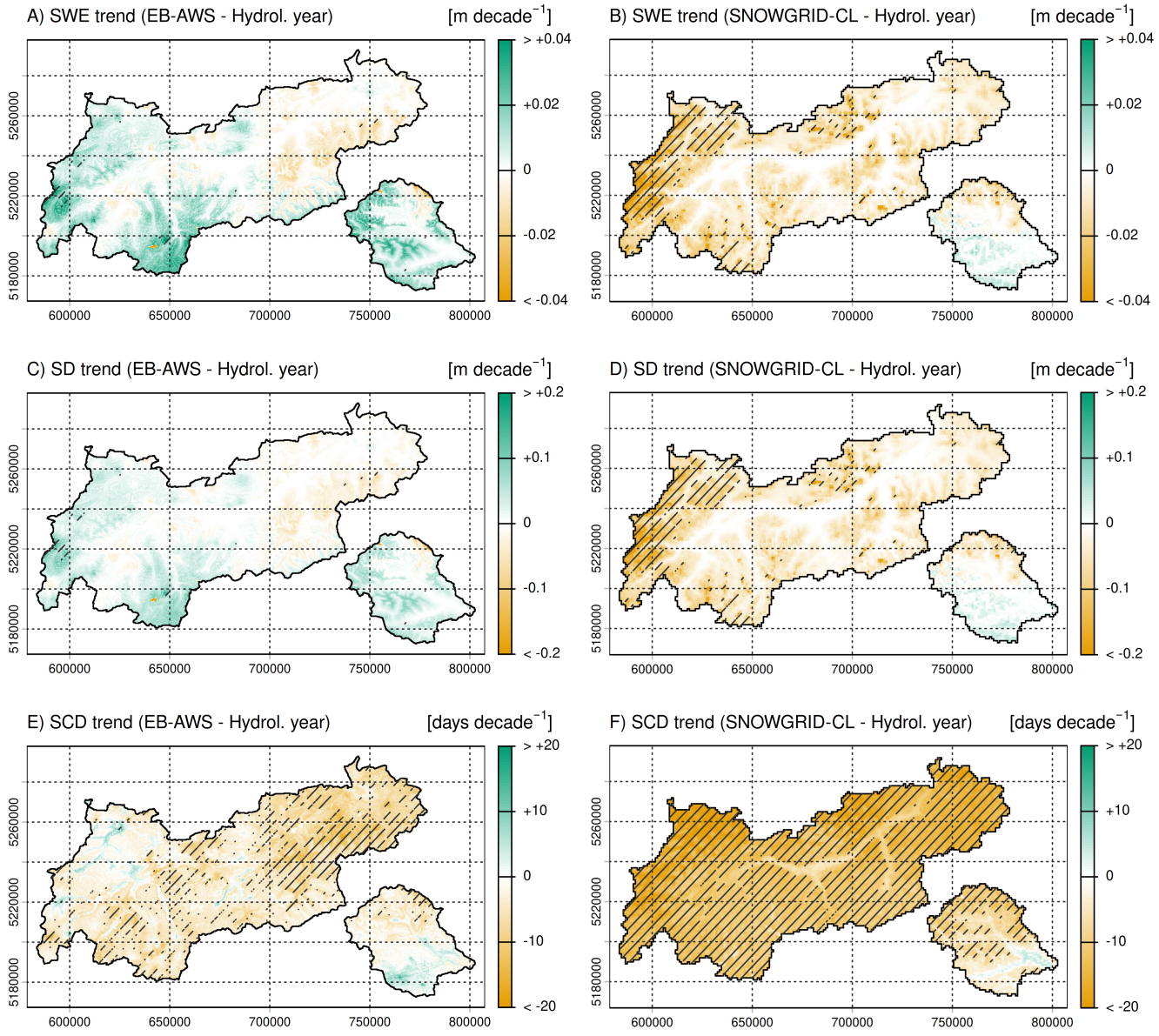

Figure 7. Trend maps of mean annual snow water equivalent (SWE; A, B), snow depth (SD; C, D), and snow cover duration (SCD; E, F) for Tyrol, Austria, for the period from October 1990 to September 2023. Trends are calculated over the full hydrological year. Results are derived from openAMUNDSEN (EB-AWS) (left column) and SNOWGRID-CL (right column). Hatching denotes statistically significant trends ($p<0.05$).

425 lations and observations can likely be attributed to a local misrepresentation of lateral snow redistribution and to the relatively coarse spatial resolution of the models, which limits their ability to resolve fine-scale topographic features. For this reason,

https://doi.org/10.5194/egusphere-2026-7224
Preprint. Discussion started: 27 November 2026
© Author(s) 2026. CC BY 4.0 License.

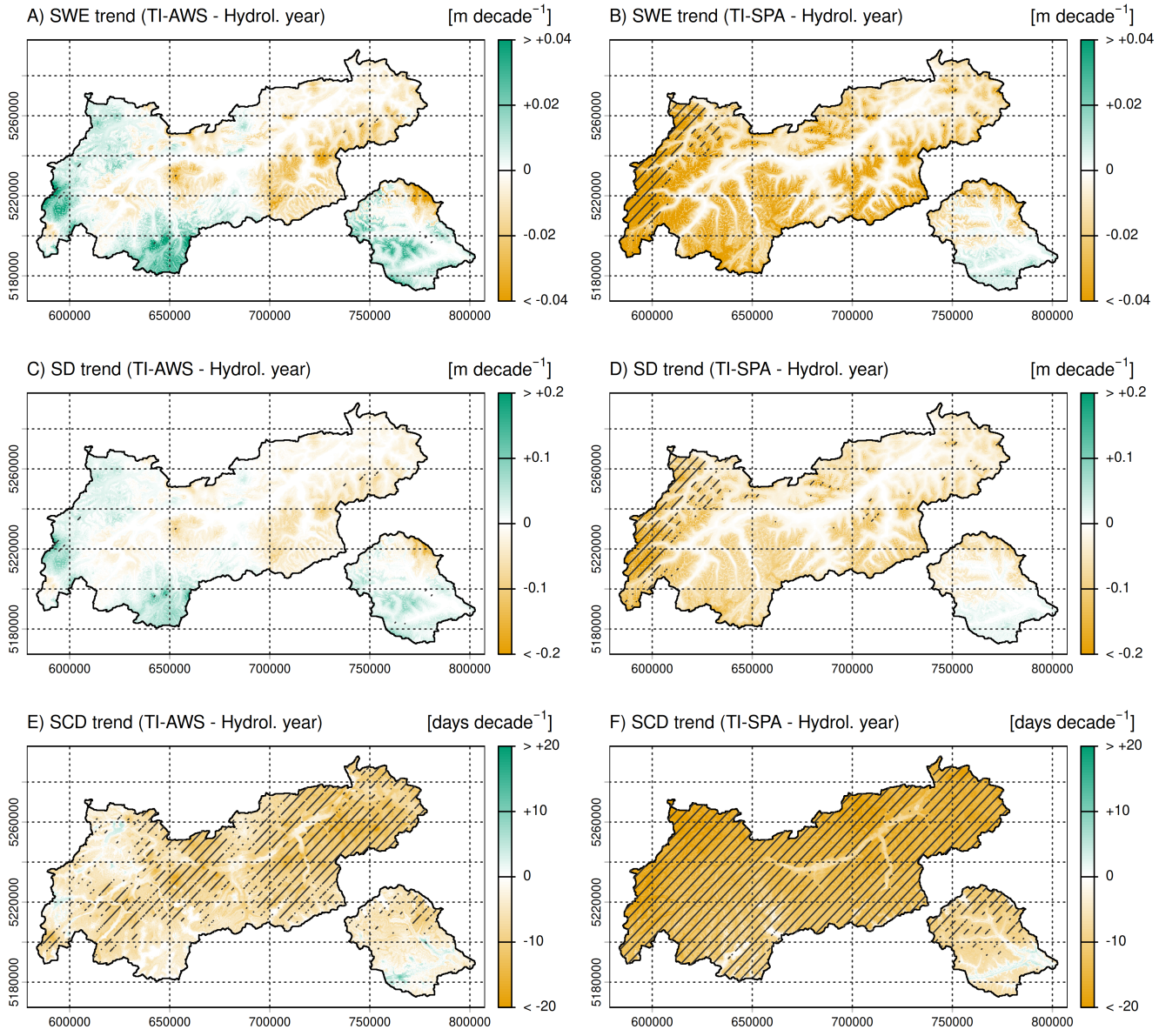

Figure 8. Trend maps of mean annual snow water equivalent (SWE; A, B), snow depth (SD; C, D), and snow cover duration (SCD; E, F) for Tyrol, Austria, for the period from October 1990 to September 2023. Trends are calculated over the full hydrological year. Results are derived from openAMUNDSEN (TI-AWS) (left column) and openAMUNDSEN (TI-SPA) (right column). Hatching denotes statistically significant trends ($p<0.05$).

comparisons between point measurements and simulated grid cell values should be interpreted with caution. The satellite-based evaluation suggests that openAMUNDSEN performs better, reproducing the seasonal evolution of snow cover more

https://doi.org/10.5194/egusphere-2026-7224
Preprint. Discussion started: 27 November 2026
© Author(s) 2026. CC BY 4.0 License.

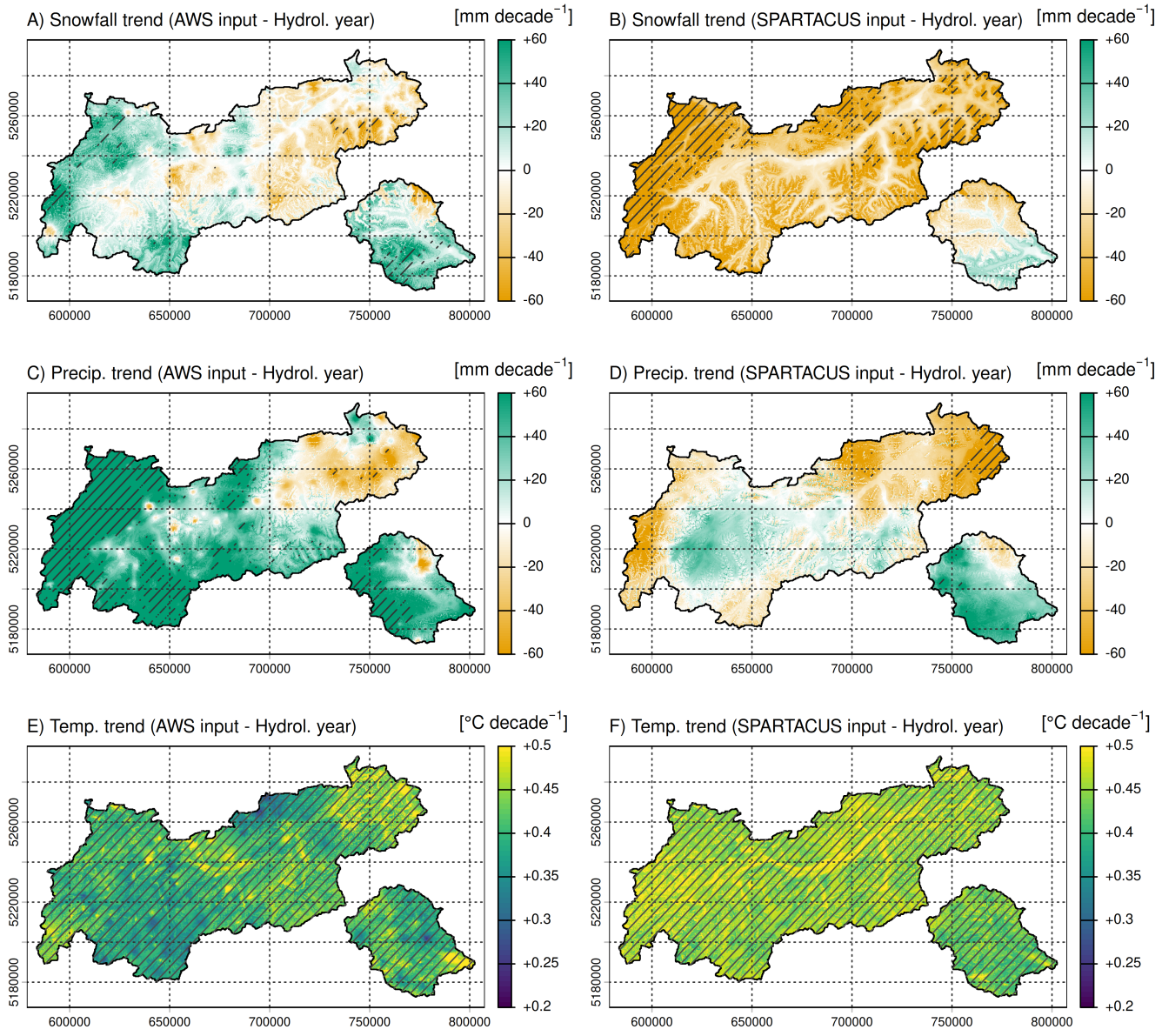

Figure 9. Trend maps of annual snowfall (A, B), precipitation (C, D), and air temperature (E, F) in Tyrol, Austria, for the period from October 1990 to September 2023. Trends are calculated over full the hydrological year. Results are based on recordings from automatic weather stations (AWS) interpolated with openAMUNDSEN (left column) and SPARTACUS v.2.1 (right column). Hatching denotes statistically significant trends ($p<0.05$).

accurately, particularly during the snowmelt season. SNOWGRID-CL tends to overestimate snow cover in Tyrol in late spring and early summer. Our findings show that evaluations based on station measurements and satellite data are not interchangeable.

https://doi.org/10.5194/egusphere-2026-7224
Preprint. Discussion started: 27 November 2026
© Author(s) 2026. CC BY 4.0 License.

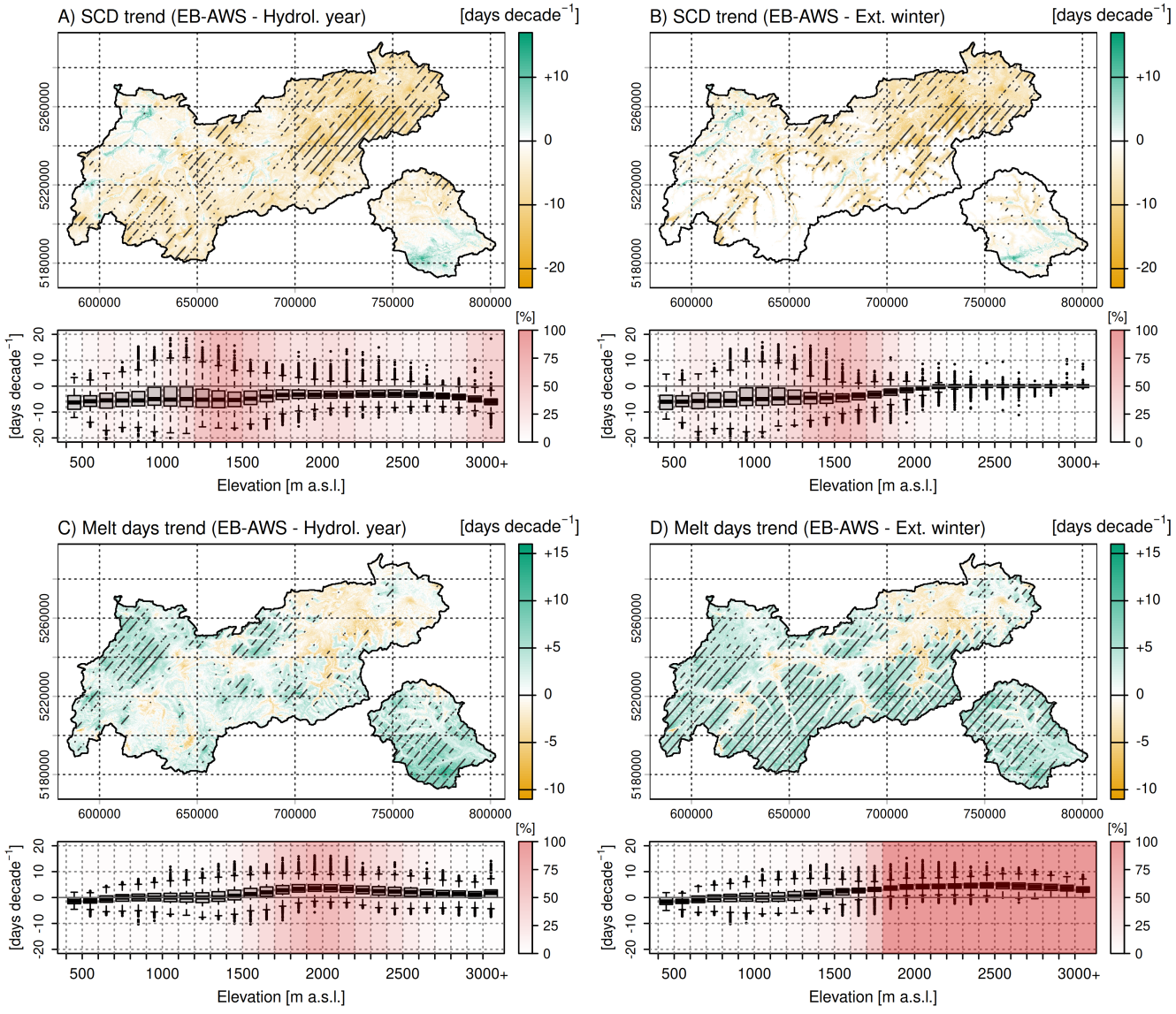

Figure 10. Trend maps of snow cover duration (SCD) and melt days calculated for the hydrological year (A, C) and the extended winter season, from November to April (B, D) derived from openAMUNDSEN (EB-AWS). Hatching indicates statistically significant trends ($p<0.05$). Below each map, results aggregated into 100 m elevation bands are shown, with all grid cells above 3,000 m a.s.l. combined into a single elevation band. Red colours indicate the percentage of grid cells within each elevation band that exhibit a statistically significant trend.

Rather, they provide complementary information and should both be conducted whenever the respective datasets are available (e.g. Warscher et al., 2013; Hanzer et al., 2016; Storebakken et al., 2025).

https://doi.org/10.5194/egusphere-2026-7224
Preprint. Discussion started: 27 November 2026
© Author(s) 2026. CC BY 4.0 License.

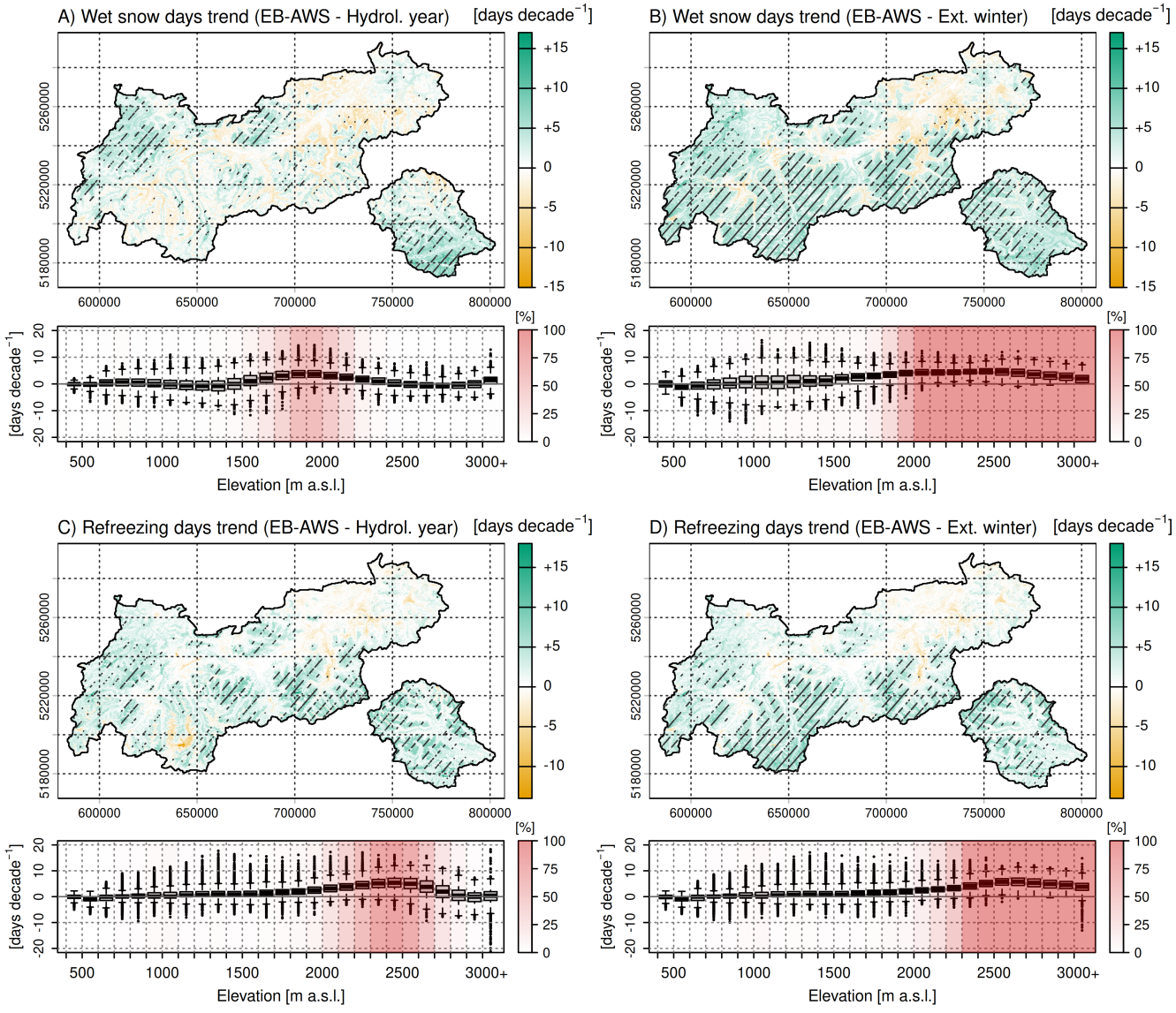

Figure 11. Trend maps of wet snow days and refreezing days calculated for the hydrological year (A, C) and the extended winter season, from November to April (B, D) derived from openAMUNDSEN (EB-AWS). Hatching indicates statistically significant trends ($p<0.05$). Below each map, results aggregated into 100 m elevation bands are shown, with all grid cells above 3,000 m a.s.l. combined into a single elevation band. Red colours indicate the percentage of grid cells within each elevation band that exhibit a statistically significant trend.

5.2 Snow cover trends and data uncertainty

The good agreement between openAMUNDSEN (EB-AWS) and SNOWGRID-CL in identifying snow-rich and snow-poor years suggests that both simulations capture the main features of interannual snow variability across the region. Both SD

https://doi.org/10.5194/egusphere-2026-7224
Preprint. Discussion started: 27 November 2026
© Author(s) 2026. CC BY 4.0 License.

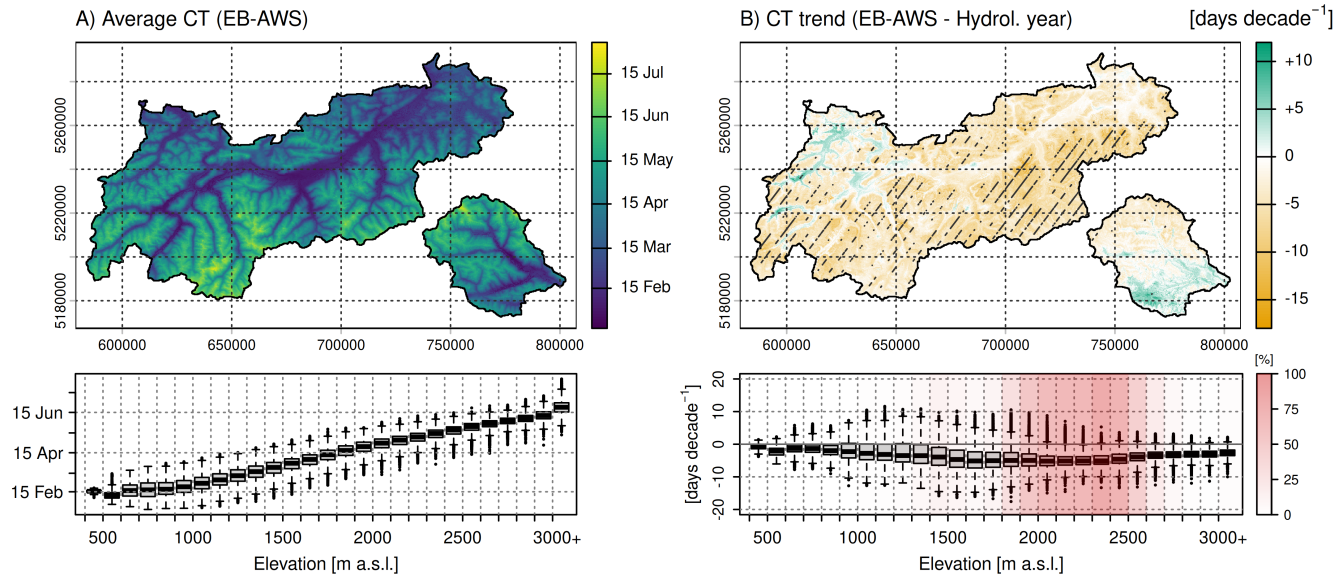

Figure 12. Map of average centre timing of meltwater production (CT; A) and trends in CT (B) in Tyrol, Austria, from October 1990 to September 2023, derived from openAMUNDSEN (EB-AWS). Hatching in panel B denotes statistically significant trends ($p<0.05$). Below each map, results aggregated into 100 m elevation bands are shown, with all grid cells above 3,000 m a.s.l. combined into a single elevation band. In the bottom plot of panel B, red colours indicate the percentage of grid cells within each elevation band exhibiting a statistically significant trend.

and SWE exhibit pronounced interannual variability, highlighting substantial year-to-year fluctuations in snow accumulation. Despite this overall agreement, systematic differences emerge between the two simulations: openAMUNDSEN (EB-AWS) tends to simulate lower SD but higher SWE than SNOWGRID-CL, as reflected in both the long-term spatial fields and the domain-average time series (Fig. 5, 6). This discrepancy suggests higher bulk snow densities in EB-AWS and may indicate differences in how the two modelling approaches represent liquid water retention and refreezing.

openAMUNDSEN (EB-AWS) and SNOWGRID-CL also yield different results in terms of snow trends. The additional simulation experiments (TI-AWS and TI-SPA) suggest that these discrepancies are primarily driven by differences in the meteorological forcing and are further amplified by differences in model complexity. This finding is consistent with previous studies identifying meteorological input data as the primary source of uncertainty in snow modelling, followed by model structure and parameter selection (Magnusson et al., 2015; Günther et al., 2019). The two meteorological datasets employed in the snow simulations (AWS-based and SPARTACUS) were also compared by Rottler et al. (2026a), who reported generally good agreement in terms of sub-seasonal dynamics. Our analyses confirm that both input datasets indicate a strong regional warming signal. However, temperature trends tend to be slightly more pronounced in SPARTACUS than in the AWS-based dataset (Fig. 9 E, F). In contrast, precipitation trends are generally weak and mostly not statistically significant in either dataset, although their spatial patterns differ, with some regions exhibiting tendencies of opposite sign. These discrepancies likely reflect differences in the

https://doi.org/10.5194/egusphere-2026-7224
Preprint. Discussion started: 27 November 2026
© Author(s) 2026. CC BY 4.0 License.

underlying observations and interpolation methods. Because our AWS-based dataset incorporates observations from multiple providers beyond GeoSphere Austria, it includes more AWS temperature records than the ones used in SPARTACUS (Hiebl and Frei, 2016), particularly at high elevations. In recent decades, high-elevation temperature records show weaker warming trends than those at lower elevations, particularly during winter (Rottler et al., 2026a). Consequently, the higher proportion of high-elevation AWS records in the station-based dataset may lead to a lower estimated regional temperature trend. For precipitation, the number of AWS within the study area is comparable between the two datasets (Hiebl and Frei, 2018). However, SPARTACUS incorporates more observations from AWS located in surrounding regions and complements the AWS time series with data from precipitation totalisers. These additional observations help constrain the monthly background fields, to which daily anomalies derived from AWS measurements are added. The inclusion of these additional data sources in SPARTACUS may result in a more robust representation of precipitation patterns and their long-term evolution. Determining which dataset provides the more realistic representation of meteorological trends is difficult and beyond the scope of this study. Nonetheless, our results demonstrate that even seemingly small differences in temperature and precipitation trends can lead to substantially different estimates of snow cover evolution. This finding highlights the strong sensitivity of snow models to meteorological forcing and emphasizes the need for particular caution when interpreting model-derived snow trend estimates.

5.3 Snow cover trends and analytical uncertainty

Another factor contributing to the uncertainty of the trend analysis is the relatively short investigation period of 33 years, which was mainly constrained by the availability of hourly meteorological observations. Over such a time span, the large interannual variability makes it difficult to detect coherent and statistically significant trends. This difficulty has been highlighted by several previous studies (Hüsler et al., 2014; Beaumet et al., 2021; Marty et al., 2017). Using satellite records, Hüsler et al. (2014) estimated that approximately 61 years of observations are needed to robustly detect significant snow cover trends given the observed natural variability. Our analysis of domain-average SD and SWE indicates that interannual variations exceeding 100 % are readily possible (Fig. 5). Furthermore, the significance of trends derived from model simulations depends not only on the intrinsic variability of snowfall but also on the snow variable investigated and model biases affecting results. In this study, SCD exhibits some of the strongest trends, with maximum magnitudes of around 20 days decade^{-1}. However, biases in SCD can be substantial and vary by year, season, and elevation. Despite numerous sources of uncertainty, our results still provide a valuable indication on the most likely directions and spatial patterns of the changes in snow conditions. The results of the openAMUNDSEN (EB-AWS) simulation indicate spatially heterogeneous trends in SD and SWE, with both increasing and decreasing tendencies occurring across the study area, although these tendencies are generally not statistically significant. SCD show a more widespread tendency towards decreasing values, albeit with statistical significance limited to specific areas. Overall, these findings align with several studies suggesting a relative stabilization with strong interannual variability of high Alpine snow cover following the marked decline observed during the late 1980s (Colombo et al., 2022; Hüsler et al., 2014; Beaumet et al., 2021; Rumpf et al., 2022; Marty et al., 2017).

https://doi.org/10.5194/egusphere-2026-7224
Preprint. Discussion started: 27 November 2026
© Author(s) 2026. CC BY 4.0 License.

5.4 Snowpack processes

Analysis of trends in internal snowpack processes derived from energy-balance-based openAMUNDSEN simulation suggests widespread and statistically significant changes in the frequency of melt days, refreezing days, and the presence of wet snow (Fig. 10, 11). Together, these findings provide a coherent picture of potential snowpack evolution in Tyrol over the 33-year study period. Surface snowmelt episodes became more frequent, particularly during the extended winter season. At lower elevations (below approximately 1,700 m a.s.l.), this increased melt activity likely contributed to the decrease in SCD. At higher elevations, however, the changes appear to be primarily qualitative rather than quantitative: although SCD did not decline significantly, the snowpack was increasingly influenced by melt-related processes. From approximately 1,700 m a.s.l. upward, our simulations indicate an increasing frequency of wet snow conditions. At elevations above approximately 2,200 m a.s.l., melt episodes were also increasingly followed by refreezing. Spatial patterns in CT trends reflect changes in both SCD and the frequency of snowmelt events. Earlier CT may result from a shorter SCD, but it may also reflect more frequent melt episodes that advance the timing of bulk meltwater release without substantially shortening the overall snow cover period. These results are consistent with the findings of Marty et al. (2023), who reported a general increase in winter snowmelt episodes across the Swiss Alps based on snow station observations. Similar changes have also been reported in western North America, where Musselman et al. (2021) identified increasing trends in winter snowmelt at several monitoring stations. Our analysis of wet snow conditions and refreezing processes was motivated by the apparent discrepancy between the pronounced increase in air temperature and the comparatively weak trends found in conventional snow metrics when using the energy balance approach of openAMUNDSEN. By examining internal snowpack processes, we detected a strong signal of change that was not evident from SCD alone. These findings highlight the need for further physically based snow model applications for investigating changes in snowpack properties and processes, including liquid water storage and refreezing, which remain difficult to investigate from observations alone. Satellite-based wet snow maps from the Sentinel-1 including their assimilation into snow hydrological models may offer a promising path toward improving the representation and understanding of liquid water retention and refreezing in snow cover evolution (Cluzet et al., 2024; Rottler et al., 2024; Wagner et al., 2026).

6 Conclusions

In this study, we used the snow-hydrological model openAMUNDSEN to investigate the snow cover evolution in Tyrol (Austria) from October 1990 to September 2023. The model was forced with an AWS-based meteorological dataset that combined measurements from different data providers. To ensure high quality and consistent model input, the AWS dataset underwent thorough quality control and gap filling. Using the energy balance scheme of openAMUNDSEN, we simulated the snow cover evolution and evaluated the results against in situ SD measurements and satellite-derived snow cover observations. The good agreement between simulations and observations demonstrated that openAMUNDSEN provides a suitable computational framework for investigating seasonal snow cover dynamics in the study area.

We then used the results of the energy-balance-based openAMUNDSEN simulation to compute trends in SD, SWE, and SCD. No statistically significant trends were detected in SD or SWE over the 33-year study period, whereas SCD exhibited

https://doi.org/10.5194/egusphere-2026-7224
Preprint. Discussion started: 27 November 2026
© Author(s) 2026. CC BY 4.0 License.

an overall decreasing tendency. These findings are consistent with previous studies of snow trends in high-Alpine regions over comparable time periods. The detection of significant trends is hindered by the strong interannual variability, suggesting that longer investigation periods than the 33 years considered here may be required to reliably identify long-term changes. We additionally compared the trends from our simulation to those derived from SNOWGRID-CL, a snow model developed by GeoSphere Austria which is widely used in snow-hydrological studies in the region. SNOWGRID-CL employs an enhanced temperature-index approach and is forced with the SPARTACUS meteorological dataset. The comparison revealed discrepancies in the trends of all three variables. Further model experiments using the temperature-index snowmelt scheme implemented in openAMUNDSEN suggested that these discrepancies are primarily attributable to differences in meteorological forcing and further amplified by differences in model complexity.

Finally, we examined changes in internal snowpack processes using the energy-balance simulation results. The analysis revealed significant increases in surface snowmelt and refreezing activity, as well as the occurrence of wet snow conditions, particularly during the extended winter season. These changes are most pronounced at higher elevations, where simulated decreasing trends in SCD are weaker.

Our results underscore the importance of high-quality meteorological forcing for snow modelling in complex high-Alpine terrain, as even seemingly small differences in temperature and precipitation input can substantially affect simulated snow trends. Improving the characterization of precipitation for the higher-altitude regions, where observations are sparse, therefore remains an important priority for further research. In addition, our results highlight the opportunities of a physically based representation of snowpack processes in climate change impact studies, in particular liquid water retention and refreezing inside the snowpack. Incorporating these processes can provide important additional insights into snow cover changes in high-Alpine terrain.

Code and data availability. The openAMUNDSEN model source code including sample data and instruction on how to install and run the model is available on GitHub (https://github.com/openamundsen/openamundsen, last access: 03 November 2026; (Hanzer et al., 2024)). The model openAMUNDSEN set-up for Tyrol (Austria) including model configuration files with all parameter settings, input grids, yearly output maps for temperature, precipitation, snowfall, snow depth, snow water equivalent, snow cover duration, melt days, wet snow days, refreezing days and centre timing is available at https://doi.org/10.23728/b2share.v0kpd-dk389. Processed meteorological station data from GeoSphere Austria are included in the repository. Station data from HD Tirol and LWD Tirol can be provided upon request. Meteorological station data from TIWAG may be directly requested from the company.

Author contributions. EB processed the station data and conducted the snow model simulations using openAMUNDSEN. With support from ER, EB prepared the first draft of the manuscript and produced the figures. US developed the original AMUNDSEN snow model, provided supervision within the framework of the VecParClim project, and offered valuable comments and suggestions during manuscript preparation. All authors contributed continuously to discussions of the research objectives, study design, and modelling results.

https://doi.org/10.5194/egusphere-2026-7224
Preprint. Discussion started: 27 November 2026
© Author(s) 2026. CC BY 4.0 License.

Competing interests. The authors declare that they have no conflict of interest.

Acknowledgements. We thank GeoSphere Austria, HD Tirol, TIWAG, LWD Tirol and LWD Bayern for the provision of meteorological and snow station data. This study was conducted within the framework of the VecParClim project (Project-No. FO999913123) which is funded by the Austrian Climate Research Programme (ACRP). Elena Bertazza receives funding for her PhD from this project. Furthermore, we thank the German Aerospace Center (DLR) for the provision of the 'Global SnowPack' data. In addition, this research has been supported by the International Network for Alpine Research Catchment Hydrology (INARCH) and the Long-Term Socio-Ecological Research (LTSER) platform of the Tyrolean Alps which is part of the national and international long-term ecological research networks of LTER-Austria, LTER Europe and ILTER. We used GPT-5.6 Terra (from Academic AI offered by the University of Innsbruck and based on OpenAI's ChatGPT, last access: 12/11/2026) to improve language and grammar. It was solely used to suggest rephrasing of existing text, mainly single sentences. No content, analyses or interpretations were generated by the tool. All text was reviewed and edited by the authors, who take full responsibility for the manuscript.

https://doi.org/10.5194/egusphere-2026-7224
Preprint. Discussion started: 27 November 2026
© Author(s) 2026. CC BY 4.0 License.

Appendix A: Snow and meteorological trends over the extended winter season

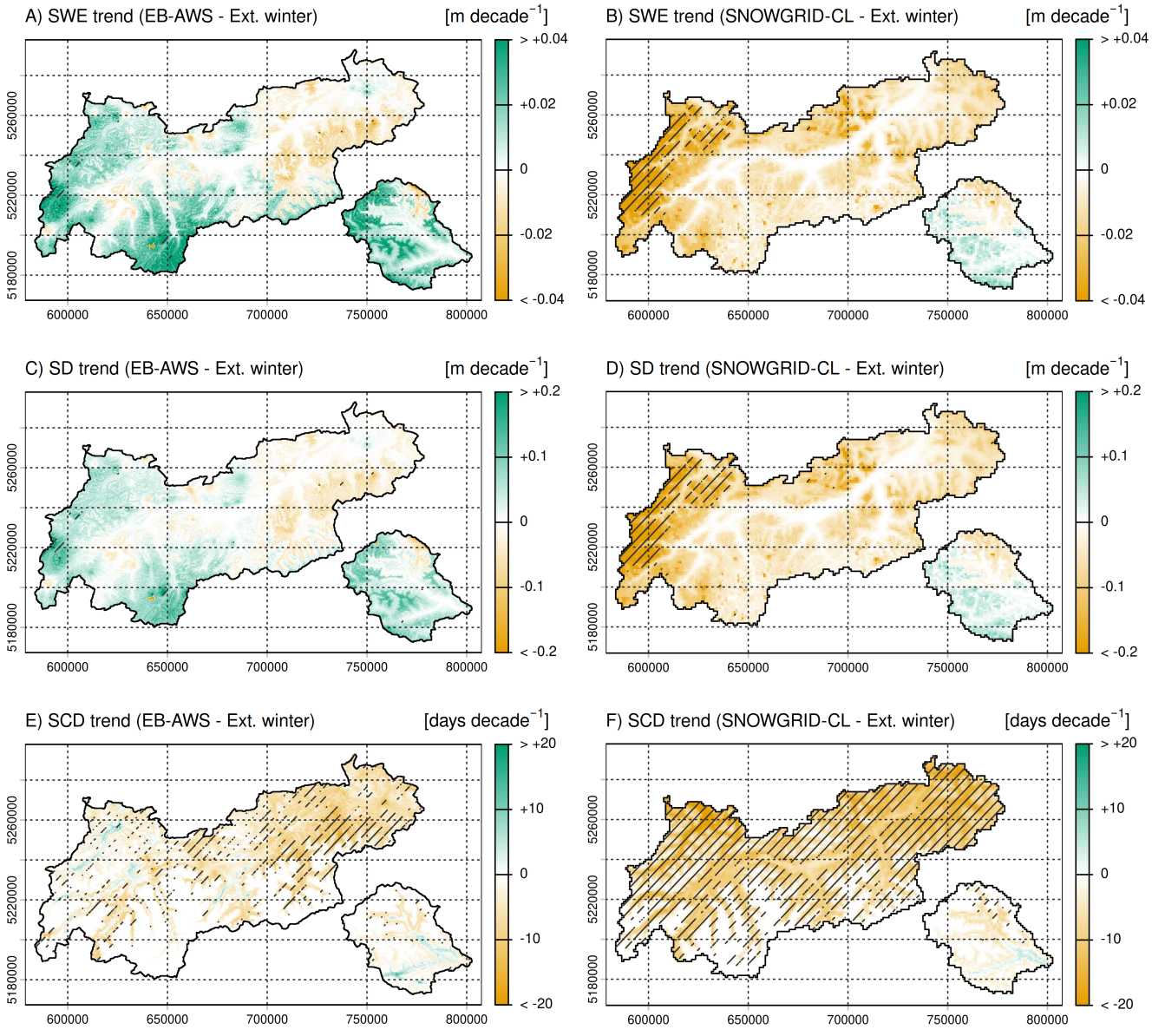

Figure A1. Trend maps of mean snow water equivalent (SWE; A, B), snow depth (SD; C, D), and snow cover duration (SCD; E, F) in Tyrol, Austria for the period 1990 to 2023. Trends are calculated over the extended winter season (November - April). Results are derived from openAMUNDSEN (EB-AWS) (left column) and SNOWGRID-CL (right column). Hatching denotes statistically significant trends ($p<0.05$).

https://doi.org/10.5194/egusphere-2026-7224
Preprint. Discussion started: 27 November 2026
© Author(s) 2026. CC BY 4.0 License.

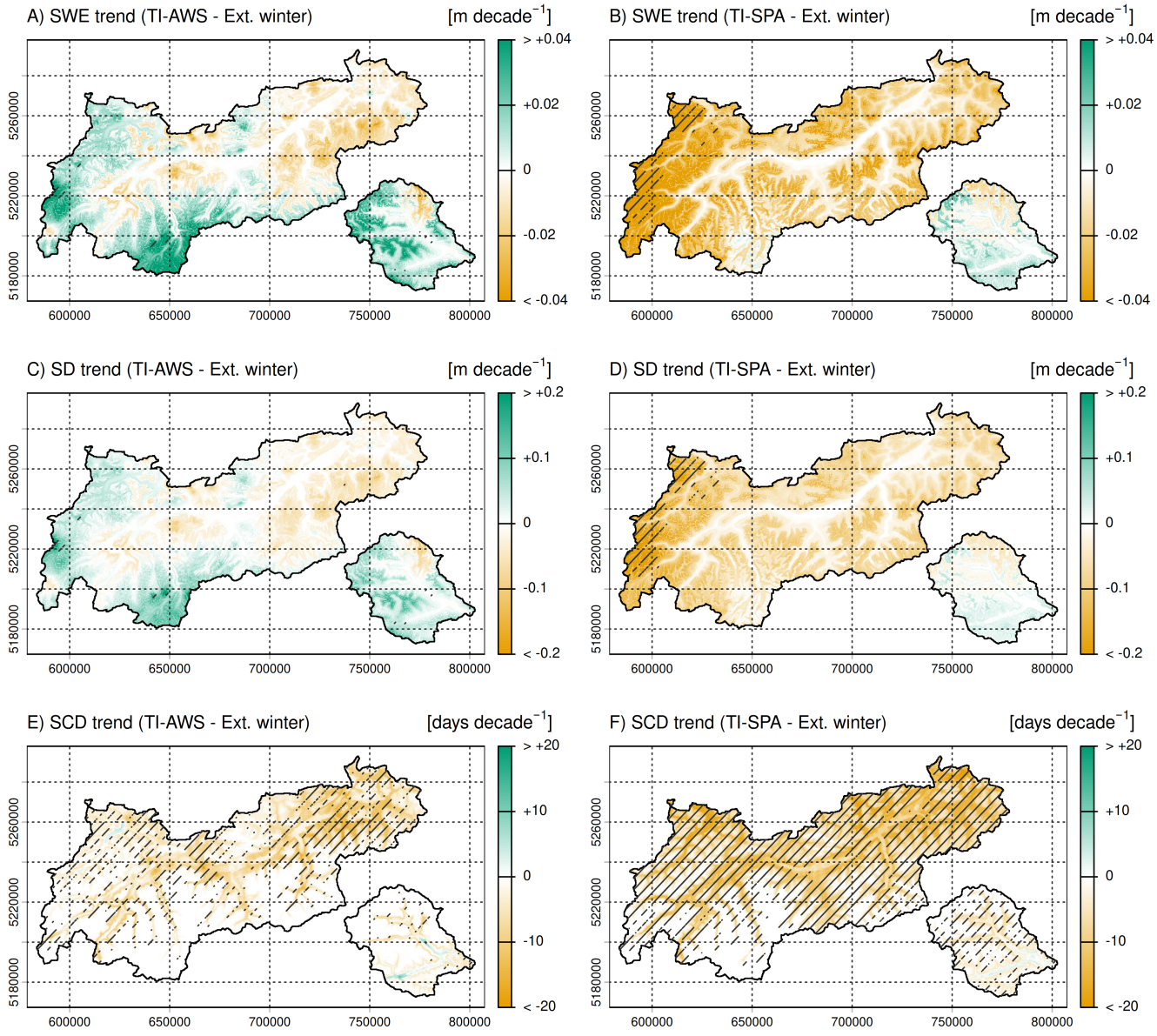

Figure A2. Trend maps of mean annual snow water equivalent (SWE; A, B), snow depth (SD; C, D), and snow cover duration (SCD; E, F) in Tyrol, Austria for the period 1990 to 2023. Trends are calculated over the extended winter season (November - April). Results are derived from openAMUNDSEN (TI-AWS) (left column) and openAMUNDSEN (TI-SPA) (right column). Hatching denotes statistically significant trends ($p<0.05$).

https://doi.org/10.5194/egusphere-2026-7224
Preprint. Discussion started: 27 November 2026
© Author(s) 2026. CC BY 4.0 License.

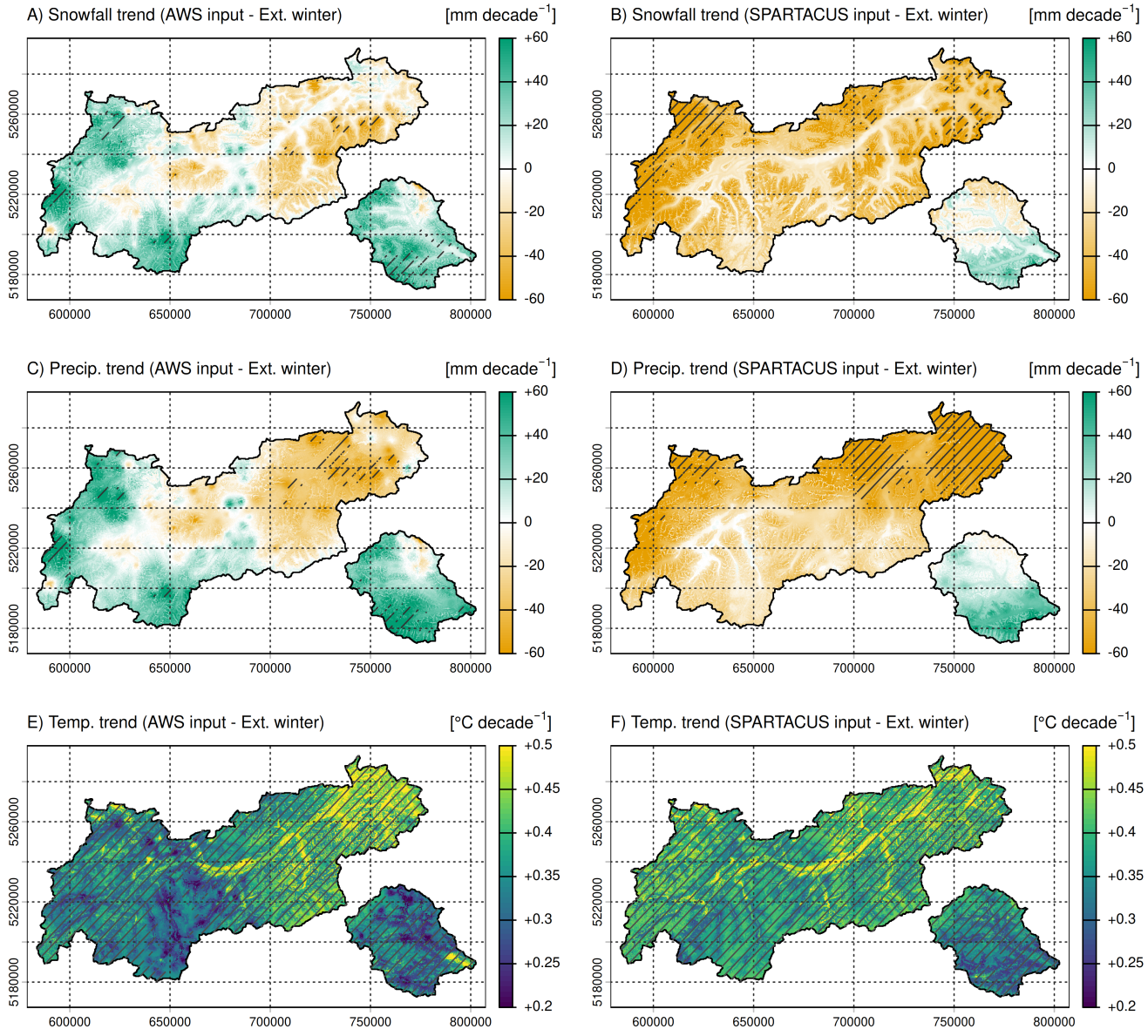

Figure A3. Trend maps of annual snowfall (A, B), precipitation (C, D), and air temperature (E, F) in Tyrol, Austria, for the period 1990 to 2023. Trends are calculated over the extended winter season (November - April). Results are based on station observations interpolated with openAMUNDSEN (left column) and SPARTACUS v.2.1 (right column). Hatching denotes statistically significant trends ($p<0.05$).

References

560 Aberle, R., Enderlin, E., O'Neel, S., Florentine, C., Sass, L., Dickson, A., Marshall, H.-P., and Flores, A.: Automated snow cover detection on mountain glaciers using spaceborne imagery and machine learning, The Cryosphere, 19, 1675–1693, https://doi.org/10.5194/tc-19-1675-2025, 2025.

https://doi.org/10.5194/egusphere-2026-7224
Preprint. Discussion started: 27 November 2026
© Author(s) 2026. CC BY 4.0 License.

Abram, N., Gattuso, J.-P., Prakash, A., Cheng, L., Chidichimo, M. P., Crate, S., Enomoto, H., Garschagen, M., Gruber, N., Harper, S., Holland, E., Kudela, R. M., Rice, J., Steffen, K., and von Schuckmann, K.: Framing and Context of the Report, in: IPCC Special Report on the Ocean and Cryosphere in a Changing Climate, edited by Pörtner, H.-O., Roberts, D. C., Masson-Delmotte, V., Zhai, P., Tignor, M., Poloczanska, E., Mintenbeck, K., Alegría, A., Nicolai, M., Okem, A., Petzold, J., Rama, B., and Weyer, N. M., pp. 73–129, Cambridge University Press, Cambridge, UK and New York, NY, USA, https://doi.org/10.1017/9781009157964.003, 2019.

Alejo-Sanchez, L. E., Márquez-Grajales, A., Salas-Martínez, F., Franco-Arcega, A., López-Morales, V., Acevedo-Sandoval, O. A., González-Ramírez, C. A., and Villegas-Vega, R.: Missing data imputation of climate time series: A review, MethodsX, 15, 103 455, 2025.

Anderson, E. A.: A point energy and mass balance model of a snow cover., Stanford University, https://repository.library.noaa.gov/view/noaa/6392/noaa_6392_DS1.pdf, 1976.

Auer, I., Böhm, R., Jurkovic, A., Lipa, W., Orlik, A., Potzmann, R., Schöner, W., Ungersböck, M., Matulla, C., Briffa, K., Jones, P., Efthymiadis, D., Brunetti, M., Nanni, T., Maugeri, M., Mercalli, L., Mestre, O., Moisselin, J.-M., Begert, M., Müller-Westermeier, G., Kveton, V., Bochnicek, O., Stastny, P., Lapin, M., Szalai, S., Szentimrey, T., Cegnar, T., Dolinar, M., Gajic-Capka, M., Zaninovic, K., Majstorovic, Z., and Nieplova, E.: HISTALP—historical instrumental climatological surface time series of the Greater Alpine Region, International Journal of Climatology, 27, 17–46, https://doi.org/10.1002/joc.1377, 2007.

Beaumet, J., Ménégoz, M., Morin, S., Gallée, H., Fettweis, X., Six, D., Vincent, C., Wilhelm, B., and Anquetin, S.: Twentieth century temperature and snow cover changes in the French Alps, Regional Environmental Change, 21, 114, https://doi.org/10.1007/s10113-021-01830-x, 2021.

Beniston, M., Farinotti, D., Stoffel, M., Andreassen, L. M., Coppola, E., Eckert, N., Fantini, A., Giacona, F., Hauck, C., Huss, M., Huwald, H., Lehning, M., López-Moreno, J.-I., Magnusson, J., Marty, C., Morán-Tejéda, E., Morin, S., Naaim, M., Provenzale, A., Rabatel, A., Six, D., Stötter, J., Strasser, U., Terzago, S., and Vincent, C.: The European mountain cryosphere: a review of its current state, trends, and future challenges, The Cryosphere, 12, 759–794, https://doi.org/10.5194/tc-12-759-2018, 2018.

Bertoldi, G., Bozzoli, M., Crespi, A., Matiu, M., Giovannini, L., Zardi, D., Majone, B., et al.: Diverging snowfall trends across months and elevation in the northeastern Italian Alps, International Journal of Climatology, 2023, 2794–2819, https://doi.org/10.1002/joc.8002, 2023.

Bormann, K. J., Brown, R. D., Derksen, C., and Painter, T. H.: Estimating snow-cover trends from space, Nature Climate Change, 8, 924–928, https://doi.org/10.1038/s41558-018-0318-3, 2018.

Bozzoli, M., Crespi, A., Matiu, M., Majone, B., Giovannini, L., Zardi, D., Brugnara, Y., Bozzo, A., Berro, D. C., Mercalli, L., and Bertoldi, G.: Long-term snowfall trends and variability in the Alps, International Journal of Climatology, 44, 4571–4591, https://doi.org/10.1002/joc.8597, 2024.

Bronaugh, D. and Werner, A.: Zyp: Zhang + Yue-Pilon Trends Package, https://doi.org/10.32614/CRAN.package.zyp, R package version 0.11-1, 2023.

Cluzet, B., Magnusson, J., Quéno, L., Mazzotti, G., Mott, R., and Jonas, T.: Exploring how Sentinel-1 wet-snow maps can inform fully distributed physically based snowpack models, The Cryosphere, 18, 5753–5767, https://doi.org/10.5194/tc-18-5753-2024, 2024.

Colombo, N., Valt, M., Romano, E., Salerno, F., Godone, D., Cianfarra, P., Freppaz, M., Maugeri, M., and Guyennon, N.: Long-term trend of snow water equivalent in the Italian Alps, Journal of Hydrology, 614, 128 532, https://doi.org/10.1016/j.jhydrol.2022.128532, 2022.

Demil, G., Torabi Haghighi, A., Klöve, B., and Oussalah, M.: Advances in Image-Based Estimation of Snow Hydrology Parameters: A Systematic Literature Review, EGUsphere, pp. 1–34, https://doi.org/10.5194/egusphere-2024-1158, 2024.

DeWalle, D. R. and Rango, A.: Principles of snow hydrology, Cambridge University Press, https://doi.org/10.1017/CBO9780511535673, 2008.

https://doi.org/10.5194/egusphere-2026-7224
Preprint. Discussion started: 27 November 2026
© Author(s) 2026. CC BY 4.0 License.

Dietz, A. J., Wohner, C., and Kuenzer, C.: European Snow Cover Characteristics between 2000 and 2011 Derived from Improved MODIS Daily Snow Cover Products, Remote Sensing, 4, 2432–2454, https://doi.org/10.3390/rs4082432, 2012.

Dietz, A. J., Kuenzer, C., and Dech, S.: Global SnowPack: a new set of snow cover parameters for studying status and dynamics of the planetary snow cover extent, Remote sensing letters, 6, 844–853, https://doi.org/10.1080/2150704X.2015.1084551, 2015.

Dong, C.: Remote sensing, hydrological modeling and in situ observations in snow cover research: A review, Journal of Hydrology, 561, 573–583, https://doi.org/10.1016/j.jhydrol.2018.04.027, 2018.

Dumont, M., Monteiro, D., Filhol, S., Gascoin, S., Marty, C., Hagenmuller, P., Morin, S., Choler, P., and Thuiller, W.: The European Alps in a changing climate: physical trends and impacts, Comptes Rendus. Géoscience, 357, 25–42, https://doi.org/10.5802/crgeos.288, 2025.

Durand, Y., Giraud, G., Laternser, M., Etchevers, P., Mérindol, L., and Lesaffre, B.: Reanalysis of 47 years of climate in the French Alps (1958–2005): climatology and trends for snow cover, Journal of applied meteorology and climatology, 48, 2487–2512, https://doi.org/10.1175/2009JAMC1810.1, 2009.

Edwards, A. C., Scalenghe, R., and Freppaz, M.: Changes in the seasonal snow cover of alpine regions and its effect on soil processes: a review, Quaternary international, 162, 172–181, https://doi.org/10.1016/j.quaint.2006.10.027, 2007.

Essery, R.: A factorial snowpack model (FSM 1.0), Geoscientific Model Development, 8, 3867–3876, https://doi.org/10.5194/gmd-8-3867-2015, 2015.

Flanner, M. G., Shell, K. M., Barlage, M., Perovich, D. K., and Tschudi, M.: Radiative forcing and albedo feedback from the Northern Hemisphere cryosphere between 1979 and 2008, Nature Geoscience, 4, 151–155, 2011.

GeoSphere Austria – Geological Map Service: Geological Map of Austria (Interactive Online Map), https://maps.geosphere.at/en, interactive geological map of Austria, accessed 21 February 2026, 2026.

Guijarro, J. A., López, J. A., Aguilar, E., Domonkos, P., Venema, V. K., Sigró, J., and Brunet, M.: Homogenization of monthly series of temperature and precipitation: Benchmarking results of the MULTITEST project, International Journal of Climatology, 43, 3994–4012, https://doi.org/10.1002/joc.8069, 2023.

Günther, D., Marke, T., Essery, R., and Strasser, U.: Uncertainties in snowpack simulations—Assessing the impact of model structure, parameter choice, and forcing data error on point-scale energy balance snow model performance, Water Resources Research, 55, 2779–2800, https://doi.org/10.1029/2018WR023403, 2019.

Günther, D., Hanzer, F., Warscher, M., Essery, R., and Strasser, U.: Including Parameter Uncertainty in an Intercomparison of Physically-Based Snow Models, Frontiers in Earth Science, 8, https://doi.org/10.3389/feart.2020.542599, 2020.

Hanzer, F., Helfricht, K., Marke, T., and Strasser, U.: Multilevel spatiotemporal validation of snow/ice mass balance and runoff modeling in glacierized catchments, The Cryosphere, 10, 1859–1881, https://doi.org/10.5194/tc-10-1859-2016, 2016.

Hanzer, F., Warscher, M., and Strasser, U.: openamundsen/openamundsen: v1.0.3, https://doi.org/10.5281/zenodo.13893160, 2024.

Hiebl, J. and Frei, C.: Daily temperature grids for Austria since 1961—concept, creation and applicability, Theoretical and applied climatology, 124, 161–178, https://doi.org/10.1007/s00704-015-1411-4, 2016.

Hiebl, J. and Frei, C.: Daily precipitation grids for Austria since 1961—Development and evaluation of a spatial dataset for hydroclimatic monitoring and modelling, Theoretical and applied climatology, 132, 327–345, https://doi.org/10.1007/s00704-017-2093-x, 2018.

Hiebl, J., Bourgeois, Q., and Tilg, Anna-Maria andFrei, C.: Daily sunshine grids for Austria since 1961 – combining station and satellite observations for a multi-decadal climate-monitoring dataset, Theoretical and applied climatology, 155, 8337—-8360, https://doi.org/10.1007/s00704-024-05103-5, 2024.

https://doi.org/10.5194/egusphere-2026-7224
Preprint. Discussion started: 27 November 2026
© Author(s) 2026. CC BY 4.0 License.

Hock, R., Rasul, G., Adler, C., Cáceres, B., Gruber, S., Hirabayashi, Y., Jackson, M., Kääb, A., Kang, S., Kutuzov, S., Milner, A., Molau, U., Morin, S., Orlove, B., and Steltzer, H.: High mountain areas, in: IPCC special report on the ocean and cryosphere in a changing climate, pp. 131–202, H.-O. Pörtner, DC Roberts, V. Masson-Delmotte, P. Zhai, M. Tignor, E. Poloczanska, K. Mintenbeck, A. Alegri´a, M. Nicolai, A. Okem, J. Petzold, B. Rama, N.M. Weyer (eds.), https://doi.org/10.1017/9781009157964.004., 2019.

Huerta, A., Brönnimann, S., de Luis, M., Beguería, S., and Serrano-Notivoli, R.: Enhancing daily precipitation reconstruction: An improved version of the reddPrec R package, Environmental Modelling & Software, p. 106717, https://doi.org/10.1016/j.envsoft.2025.106717, 2025.

Hüsler, F., Jonas, T., Riffler, M., Musial, J. P., and Wunderle, S.: A satellite-based snow cover climatology (1985–2011) for the European Alps derived from AVHRR data, The Cryosphere, 8, 73–90, https://doi.org/10.5194/tc-8-73-2014, 2014.

Immerzeel, W. W., Lutz, A. F., Andrade, M., Bahl, A., Biemans, H., Bolch, T., Hyde, S., Brumby, S., Davies, B., Elmore, A., et al.: Importance and vulnerability of the world's water towers, Nature, 577, 364–369, https://doi.org/10.1038/s41586-019-1822-y, 2020.

Johnston, J., Jacobs, J. M., and Cho, E.: Global snow seasonality regimes from satellite records of snow cover, Journal of Hydrometeorology, 25, 65–88, https://doi.org/10.1175/JHM-D-23-0047.1, 2024.

Jordan, R.: A one-dimensional temperature model for a snow cover: technical documentation for SNTHERM. 89., Tech. rep., https://api.semanticscholar.org/CorpusID:126628105, 1991.

Kang, M., Ichii, K., Kim, J., Indrawati, Y. M., Park, J., Moon, M., Lim, J.-H., and Chun, J.-H.: New gap-filling strategies for long-period flux data gaps using a data-driven approach, Atmosphere, 10, 568, https://doi.org/10.3390/atmos10100568, 2019.

Kendall, M. G.: Rank Correlation Methods, Charles Griffin, London, 4th edn., 1975.

Klein, G., Vitasse, Y., Rixen, C., Marty, C., and Rebetez, M.: Shorter snow cover duration since 1970 in the Swiss Alps due to earlier snowmelt more than to later snow onset, Climatic Change, 139, 637–649, https://doi.org/10.1007/s10584-016-1806-y, 2016.

Kochendorfer, J., Rasmussen, R., Wolff, M., Baker, B., Hall, M. E., Meyers, T., Landolt, S., Jachcik, A., Isaksen, K., Brækkan, R., and Leeper, R.: The quantification and correction of wind-induced precipitation measurement errors, Hydrology and Earth System Sciences, 21, 1973–1989, https://doi.org/10.5194/hess-21-1973-2017, 2017.

Körner, P., Kronenberg, R., Genzel, S., and Bernhofer, C.: Introducing Gradient Boosting as a universal gap filling tool for meteorological time series, Meteorologische Zeitschrift, 27, 369–376, https://doi.org/10.1127/metz/2018/0908, 2018.

Krinner, G., Derksen, C., Essery, R., Flanner, M., Hagemann, S., Clark, M., Hall, A., Rott, H., Brutel-Vuilmet, C., Kim, H., Ménard, C. B., Mudryk, L., Thackeray, C., Wang, L., Arduini, G., Balsamo, G., Bartlett, P., Boike, J., Boone, A., Chéruy, F., Colin, J., Cuntz, M., Dai, Y., Decharme, B., Derry, J., Ducharne, A., Dutra, E., Fang, X., Fierz, C., Ghattas, J., Gusev, Y., Haverd, V., Kontu, A., Lafaysse, M., Law, R., Lawrence, D., Li, W., Marke, T., Marks, D., Ménégoz, M., Nasonova, O., Nitta, T., Niwano, M., Pomeroy, J., Raleigh, M. S., Schaedler, G., Semenov, V., Smirnova, T. G., Stacke, T., Strasser, U., Svenson, S., Turkov, D., Wang, T., Wever, N., Yuan, H., Zhou, W., and Zhu, D.: ESM-SnowMIP: assessing snow models and quantifying snow-related climate feedbacks, Geoscientific Model Development, 11, 5027–5049, https://doi.org/10.5194/gmd-11-5027-2018, 2018.

Laternser, M. and Schneebeli, M.: Long-term snow climate trends of the Swiss Alps (1931–99), International Journal of Climatology, 23, 733–750, https://doi.org/10.1002/joc.912, 2003.

Magnusson, J., Wever, N., Essery, R., Helbig, N., Winstral, A., and Jonas, T.: Evaluating snow models with varying process representations for hydrological applications, Water Resources Research, 51, 2707–2723, https://doi.org/10.1002/2014WR016498, 2015.

Mann, H. B.: Nonparametric tests against trend, Econometrica: Journal of the econometric society, pp. 245–259, 1945.

Marsoner, T., Simion, H., Giombini, V., Egarter Vigl, L., and Candiago, S.: A detailed land use/land cover map for the European Alps macro region, Scientific Data, 10, 468, https://doi.org/10.1038/s41597-023-02344-3, 2023.

https://doi.org/10.5194/egusphere-2026-7224
Preprint. Discussion started: 27 November 2026
© Author(s) 2026. CC BY 4.0 License.

Marty, C.: Regime shift of snow days in Switzerland, Geophysical Research Letters, 35, https://doi.org/10.1029/2008GL033998, 2008.

Marty, C. and Meister, R.: Long-term snow and weather observations at Weissfluhjoch and its relation to other high-altitude observatories in the Alps, Theoretical and Applied Climatology, 110, 573–583, https://doi.org/10.1007/s00704-012-0584-3, 2012.

Marty, C., Tilg, A.-M., and Jonas, T.: Recent evidence of large-scale receding snow water equivalents in the European Alps, Journal of Hydrometeorology, 18, 1021–1031, https://doi.org/10.1175/JHM-D-16-0188.1, 2017.

Marty, C., Rohrer, M. B., Huss, M., and Stähli, M.: Multi-decadal observations in the Alps reveal less and wetter snow, with increasing variability, Frontiers in Earth Science, 11, 1165 861, https://doi.org/10.3389/feart.2023.1165861, 2023.

Matiu, M., Crespi, A., Bertoldi, G., Carmagnola, C. M., Marty, C., Morin, S., Schöner, W., Cat Berro, D., Chiogna, G., De Gregorio, L., Kotlarski, S., Majone, B., Resch, G., Terzago, S., Valt, M., Beozzo, W., Cianfarra, P., Gouttevin, I., Marcolini, G., Notarnicola, C., Petitta, M., Scherrer, S. C., Strasser, U., Winkler, M., Zebisch, M., Cicogna, A., Cremonini, R., Debernardi, A., Faletto, M., Gaddo, M., Giovannini, L., Mercalli, L., Soubeyroux, J.-M., Sušnik, A., Trenti, A., Urbani, S., and Weilguni, V.: Observed snow depth trends in the European Alps: 1971 to 2019, The Cryosphere, 15, 1343–1382, https://doi.org/10.5194/tc-15-1343-2021, 2021.

McLeod, A.: Kendall: Kendall Rank Correlation and Mann-Kendall Trend Test, https://doi.org/10.32614/CRAN.package.Kendall, R package version 2.2.1, 2022.

Monteiro, D. and Morin, S.: Multi-decadal analysis of past winter temperature, precipitation and snow cover data in the European Alps from reanalyses, climate models and observational datasets, The Cryosphere, 17, 3617–3660, https://doi.org/10.5194/tc-17-3617-2023, 2023.

Musselman, K. N., Addor, N., Vano, J. A., and Molotch, N. P.: Winter melt trends portend widespread declines in snow water resources, Nature Climate Change, 11, 418–424, https://doi.org/10.1038/s41558-021-01014-9, 2021.

Olefs, M., Koch, R., Schöner, W., and Marke, T.: Changes in snow depth, snow cover duration, and potential snowmaking conditions in Austria, 1961–2020—a model based approach, Atmosphere, 11, https://doi.org/10.3390/atmos11121330, 2020.

Pellicciotti, F., Brock, B., Strasser, U., Burlando, P., Funk, M., and Corripio, J.: An enhanced temperature-index glacier melt model including the shortwave radiation balance: development and testing for Haut Glacier d'Arolla, Switzerland, Journal of glaciology, 51, 573–587, https://doi.org/10.3189/172756505781829124, 2005.

Pirazzini, R., Leppänen, L., Picard, G., Lopez-Moreno, J. I., Marty, C., Macelloni, G., Kontu, A., Von Lerber, A., Tanis, C. M., Schneebeli, M., et al.: European in-situ snow measurements: practices and purposes, Sensors, 18, 2016, https://doi.org/10.3390/s18072016, 2018.

Ranzi, R., Colosio, P., and Galeati, G.: Climatology of snow depth and water equivalent measurements in the Italian Alps (1967–2020), Hydrology and Earth System Sciences, 28, 2555–2578, https://doi.org/10.5194/hess-28-2555-2024, 2024.

Rasmussen, R., Baker, B., Kochendorfer, J., Meyers, T., Landolt, S., Fischer, A. P., Black, J., Thériault, J. M., Kucera, P., Gochis, D., et al.: How well are we measuring snow: The NOAA/FAA/NCAR winter precipitation test bed, Bulletin of the American Meteorological Society, 93, 811–829, https://doi.org/10.1175/BAMS-D-11-00052.1, 2012.

Reid, P. C., Hari, R. E., Beaugrand, G., Livingstone, D. M., Marty, C., Straile, D., Barichivich, J., Goberville, E., Adrian, R., Aono, Y., et al.: Global impacts of the 1980s regime shift, Global change biology, 22, 682–703, https://doi.org/10.1111/gcb.13106, 2016.

Rittger, K., Raleigh, M. S., Dozier, J., Hill, A. F., Lutz, J. A., and Painter, T. H.: Canopy adjustment and improved cloud detection for remotely sensed snow cover mapping, Water Resources Research, 56, e2019WR024 914, https://doi.org/10.1029/2019WR024914, 2020.

Roberts, D., Forrest, A., Sahoo, G., Hook, S., and Schladow, S.: Snowmelt timing as a determinant of lake inflow mixing, Water Resources Research, 54, 1237–1251, https://doi.org/10.1002/2017WR021977, 2018.

Roessler, S. and Dietz, A. J.: Development of Global Snow Cover—Trends from 23 Years of Global SnowPack, Earth, 4, 1–22, https://doi.org/10.3390/earth4010001, 2023.

https://doi.org/10.5194/egusphere-2026-7224
Preprint. Discussion started: 27 November 2026
© Author(s) 2026. CC BY 4.0 License.

Rottler, E., Bronstert, A., Bürger, G., and Rakovec, O.: Projected changes in Rhine River flood seasonality under global warming, Hydrology and Earth System Sciences, 25, 2353–2371, https://doi.org/10.5194/hess-25-2353-2021, 2021.

Rottler, E., Warscher, M., Hanzer, F., and Strasser, U.: Spatio-temporal wet snow dynamics from model simulations and remote sensing: A case study from the Rofental, Austria, Hydrological Processes, 38, e15 279, https://doi.org/10.1002/hyp.15279, 2024.

Rottler, E., Bertazza, E., Wagner, F., Meißl, G., Schellander-Gorgas, T., Schöber, J., and Strasser, U.: Station-Based Assessment of Sub-Seasonal Climate Trends in the Tyrolean Alps (Austria), International Journal of Climatology, p. e70527, https://doi.org/10.1002/joc.70527, 2026a.

Rottler, E., Storebakken, B., Warscher, M., Hanzer, F., Bertazza, E., and Strasser, U.: Assessment of snow model uncertainty in relation to the effect of a 1 °C warming using the snow modelling framework openAMUNDSEN, The Cryosphere, 20, 2351–2373, https://doi.org/10.5194/tc-20-2351-2026, 2026b.

Rumpf, S. B., Gravey, M., Brönnimann, O., Luoto, M., Cianfrani, C., Mariethoz, G., and Guisan, A.: From white to green: Snow cover loss and increased vegetation productivity in the European Alps, Science, 376, 1119–1122, https://doi.org/10.1126/science.abn6697, 2022.

Scherrer, S. C., Appenzeller, C., and Laternser, M.: Trends in Swiss Alpine snow days: The role of local-and large-scale climate variability, Geophysical Research Letters, 31, https://doi.org/10.1029/2004GL020255, 2004.

Schöner, W., Koch, R., Matulla, C., Marty, C., and Tilg, A.-M.: Spatiotemporal patterns of snow depth within the Swiss-Austrian Alps for the past half century (1961 to 2012) and linkages to climate change, International Journal of Climatology, 39, 1589–1603, https://doi.org/10.1002/joc.5902, 2019.

Sen, P. K.: Estimates of the Regression Coefficient Based on Kendall's Tau, Journal of the American Statistical Association, 63, 1379–1389, https://doi.org/10.1080/01621459.1968.10480934, 1968.

Slatyer, R. A., Umbers, K. D., and Arnold, P. A.: Ecological responses to variation in seasonal snow cover, Conservation Biology, 36, e13 727, https://doi.org/10.1111/cobi.13727, 2022.

Stekhoven, D. J. and Bühlmann, P.: MissForest—non-parametric missing value imputation for mixed-type data, Bioinformatics, 28, 112–118, https://doi.org/10.1093/bioinformatics/btr597, 2012.

Stewart, I. T., Cayan, D. R., and Dettinger, M. D.: Changes in snowmelt runoff timing in western North America under abusiness as usual'climate change scenario, Climatic Change, 62, 217–232, https://doi.org/10.1023/B:CLIM.0000013702.22656.e8, 2004.

Storebakken, B., Rottler, E., Warscher, M., and Strasser, U.: Modelling of the Seasonal Snow Cover Dynamics for Open and Forested Areas in the Berchtesgaden National Park (Germany) Using the openAMUNDSEN Mountain Snow Cover Model, Hydrological Processes, 39, e70 197, https://doi.org/10.1002/hyp.70197, 2025.

Strasser, U.: Die Modellierung Der Gebirgsschneedecke Im Nationalpark Berchtesgaden: Modelling of the Mountain Snow Cover in the Berchtesgaden National Park, Nationalparkverwaltung, 2008.

Strasser, U., Warscher, M., and Liston, G. E.: Modeling snow–canopy processes on an idealized mountain, Journal of Hydrometeorology, 12, 663–677, https://doi.org/10.1175/2011JHM1344.1, 2011.

Strasser, U., Warscher, M., Rottler, E., and Hanzer, F.: openAMUNDSEN v1.0: an open-source snow-hydrological model for mountain regions, Geoscientific Model Development, 17, 6775–6797, https://doi.org/10.5194/gmd-17-6775-2024, 2024.

Techel, F. and Pielmeier, C.: Point observations of liquid water content in wet snow–investigating methodical, spatial and temporal aspects, The Cryosphere, 5, 405–418, https://doi.org/10.5194/tc-5-405-2011, 2011.

Theil, H.: A Rank-Invariant Method of Linear and Polynomial Regression Analysis, Proceedings of the National Academy of Sciences, 53, Part I: 386–392, Part II: 521–525, Part III: 1397–1412, 1950.

https://doi.org/10.5194/egusphere-2026-7224
Preprint. Discussion started: 27 November 2026
© Author(s) 2026. CC BY 4.0 License.

Uzun, S., Tanir, T., Coelho, G. d. A., Souza de Lima, A. d., Cassalho, F., and Ferreira, C. M.: Changes in snowmelt runoff timing in the contiguous United States, Hydrological Processes, 35, e14 430, https://doi.org/10.1002/hyp.14430, 2021.

Valt, M. and Cianfarra, P.: Recent snow cover variability in the Italian Alps, Cold Regions Science and Technology, 64, 146–157, https://doi.org/10.1016/j.coldregions.2010.08.008, 2010.

Vavrus, S.: The role of terrestrial snow cover in the climate system, Climate Dynamics, 29, 73–88, https://doi.org/10.1007/s00382-007-0226-0, 2007.

Viviroli, D., Dürr, H. H., Messerli, B., Meybeck, M., and Weingartner, R.: Mountains of the world, water towers for humanity: Typology, mapping, and global significance, Water resources research, 43, https://doi.org/10.1029/2006WR005653, 2007.

Vorkauf, M., Marty, C., Kahmen, A., and Hiltbrunner, E.: Past and future snowmelt trends in the Swiss Alps: the role of temperature and snowpack, Climatic Change, 165, 44, https://doi.org/10.1007/s10584-021-03027-x, 2021.

Wagner, F., Rottler, E., and Strasser, U.: openAMUNDSEN-DA v0.9: an ensemble based snow data assimilation framework for the open source snow hydrological model openAMUNDSEN, EGUsphere, 2026, 1–30, https://doi.org/10.5194/egusphere-2026-4575, 2026.

Wang, X. L. and Swail, V. R.: Trends of Atlantic wave extremes as simulated in a 40-yr wave hindcast using kinematically reanalyzed wind fields, Journal of climate, 15, 1020–1035, https://doi.org/10.1175/1520-0442(2002)015<1020:TOAWEA>2.0.CO;2, 2002.

Warscher, M., Strasser, U., Kraller, G., Marke, T., Franz, H., and Kunstmann, H.: Performance of complex snow cover descriptions in a distributed hydrological model system: A case study for the high Alpine terrain of the Berchtesgaden Alps, Water Resources Research, 49, 2619–2637, https://doi.org/10.1002/wrcr.20219, 2013.

Warscher, M., Marke, T., Rottler, E., and Strasser, U.: Operational and experimental snow observation systems in the upper Rofental: data from 2017 to 2023, Earth System Science Data Discussions, 2024, 1–26, https://doi.org/10.5194/essd-2024-45, 2024.

Wright, M. N. and Ziegler, A.: ranger: A fast implementation of random forests for high dimensional data in C++ and R, Journal of statistical software, 77, 1–17, https://doi.org/10.18637/jss.v077.i01, 2017.

Xiao, C.-D., Wang, S.-J., and Qin, D.-H.: A preliminary study of cryosphere service function and value evaluation, Advances in climate change research, 6, 181–187, https://doi.org/10.1016/j.accre.2015.11.004, 2015.

Yokoyama, R.: Visualizing topography by openness: A new application of image processing to digital elevation models, Photogramm Eng Remote Sens, 68, 257–265, 2002.

Zhou, G., Cui, M., Wan, J., and Zhang, S.: A review on snowmelt models: progress and prospect, Sustainability, 13, 11 485, https://doi.org/10.3390/su132011485, 2021.